

© 2018 by Daniel John O'Grady. All rights reserved.

INVESTIGATION OF PELLET CLAD INTERACTION DURING LOAD-FOLLOW  
OPERATION IN A PRESSURIZED WATER REACTOR USING VERA-CS

BY

DANIEL JOHN O'GRADY

THESIS

Submitted in partial fulfillment of the requirements  
for the degree of Master of Science in Nuclear, Plasma, and Radiological Engineering  
in the Graduate College of the  
University of Illinois at Urbana-Champaign, 2018

Urbana, Illinois

Master's Committee:

Professor Tomasz Kozloski, Advisor

# **Abstract**

This is a comprehensive study of caffeine consumption by graduate students at the University of Illinois who are in the very final stages of completing their doctoral degrees. A study group of six hundred doctoral students....

*To Father and Mother.*

# Acknowledgments

This project would not have been possible without the support of many people. Many thanks to my adviser, Lawrence T. Strongarm, who read my numerous revisions and helped make some sense of the confusion. Also thanks to my committee members, Reginald Bottoms, Karin Vegas, and Cindy Willy, who offered guidance and support. Thanks to the University of Illinois Graduate College for awarding me a Dissertation Completion Fellowship, providing me with the financial means to complete this project. And finally, thanks to my husband, parents, and numerous friends who endured this long process with me, always offering support and love.

# Table of Contents

<b>List of Tables . . . . .</b>	<b>vi</b>
<b>List of Figures . . . . .</b>	<b>vii</b>
<b>List of Abbreviations . . . . .</b>	<b>viii</b>
<b>List of Symbols . . . . .</b>	<b>ix</b>
<b>Chapter 1 Introduction . . . . .</b>	<b>1</b>
1.1 Background and Motivation . . . . .	1
1.1.1 Pellet Clad Interaction . . . . .	3
1.2 Literature Review . . . . .	4
<b>Chapter 2 PWR1 . . . . .</b>	<b>15</b>
2.1 PWR 1 Model Description . . . . .	15
2.1.1 VERA-CS . . . . .	16
2.1.2 Work Flow and Modeling Strategy . . . . .	17
2.2 VERA-CS Results . . . . .	18
2.2.1 Low Power Physics Testing . . . . .	18
2.2.2 Cycle Depletion . . . . .	19
2.3 Load-Follow Operation . . . . .	21
<b>Chapter 3 Methodology . . . . .</b>	<b>24</b>
3.1 MPACT Screening Process . . . . .	24
3.2 BISON . . . . .	26
<b>Chapter 4 Results and Discussion . . . . .</b>	<b>28</b>
4.1 BISON . . . . .	28
4.1.1 Start-up Power Ramp . . . . .	28
4.1.2 Load-follow Ramp 1 . . . . .	30
4.1.3 Load-follow Ramp 2 . . . . .	33
4.1.4 Load-follow Ramp 3 . . . . .	37
4.2 Limiting Pin . . . . .	37
<b>Chapter 5 Conclusions . . . . .</b>	<b>41</b>
<b>References . . . . .</b>	<b>42</b>
<b>Vita . . . . .</b>	<b>45</b>

# List of Tables

2.1 Low Power Physics Results . . . . .	19
---	----

# List of Figures

1.1	Visualization of the hoop stress acting on the fuel cladding using the thin wall approximation [1] . . . . .	3
1.2	The Power history (left), Falcon predicted hoop stress and Falcon predicted CDI (right) for Q11/1 of the Studsvik ramp program [2] . . . . .	9
2.1	Primary physics simulator components of VERA-CS used in this work. . . . .	17
2.2	Modeling strategy to simulate load follow in PWR1 cycle 21. . . . .	18
2.3	Comparison of control rod worth of all 9 rod banks at HZP. . . . .	20
2.4	Comparison of simulated to the measured critical boron concentrations. . . . .	20
2.5	PWR1 hourly power history and predicted Axial Offset (AO) during the first 30 days of plant operation . . . . .	23
4.1	BISON predicted maximum clad hoop stress [ $MPa$ ] (top) and minimum gap distance [ $\mu m$ ] (bottom) for start-up power ramp. . . . .	29
4.2	BISON predicted maximum clad hoop stress [ $MPa$ ] (top) and minimum gap distance [ $\mu m$ ] (bottom) for the first load-follow power maneuver. . . . .	31
4.3	BISON predicted maximum clad hoop stress [ $MPa$ ] (top) and minimum gap distance [ $\mu m$ ] (bottom) for the second load-follow power maneuver. . . . .	32
4.4	BISON predicted maximum clad hoop stress [ $MPa$ ] (top) and minimum gap distance [ $\mu m$ ] (bottom) for the third load-follow power maneuver. . . . .	34
4.5	BISON predicted maximum clad hoop stress [ $MPa$ ] (top) and minimum gap distance [ $\mu m$ ] (bottom) for the forth load-follow power maneuver. . . . .	35
4.6	BISON predicted maximum clad hoop stress [ $MPa$ ] (top) and minimum gap distance [ $\mu m$ ] (bottom) for the fifth load-follow power maneuver. . . . .	36
4.7	Weighted change in linear heat rate for the first (top) and second (bottom) load-follow power maneuver. . . . .	38
4.8	Weighted change in linear heat rate for the third (top) and forth (bottom) load-follow power maneuver. . . . .	39
4.9	Weighted change in linear heat rate for the fifth (top) and forth (bottom) load-follow power maneuver. . . . .	40

# List of Abbreviations

CA            Caffeine Addict.

CD            Coffee Drinker.

# List of Symbols

$\tau$  Time taken to drink one cup of coffee.

$\mu\text{g}$  Micrograms (of caffeine, generally).

# Chapter 1

## Introduction

In the United States (U.S.), nuclear power generation has high fixed costs and low variable costs. As a result, utilities have traditionally sought to operate nuclear stations at full power from Beginning of Cycle (BOC) to End of Cycle (EOC). More recently, the deregulation of the energy market and the emergence of intermittent renewable energy sources have caused load-follow operation to become a more attractive option for nuclear generation.

The deregulation of the energy market has forced utilities to compete against each other to sell electricity within a region. The beneficiary of this competition are the customers, who are guaranteed fair prices for electricity and will not be footing the bill for an inefficient/uneconomical utility project. Nuclear stations have typically been able to economically compete within deregulated markets because the typical plant lifetime of at least 20 years allows owners to spread out the fixed costs. Recently, the low price of natural gas and government subsidized renewable energy sources, such as wind and solar, have made nuclear stations appear uneconomic.

### 1.1 Background and Motivation

In 2016, the U.S. had approximately 7% of its total electricity generation coming from wind and solar power [3]. This share is likely to increase as the U.S. continues to move away from fossil fuels and towards a "greener" energy future. As a result of this increase, in combination with the deregulation of the energy market, the price of electricity has become volatile. At certain times, the price of selling electricity within a region can even become negative, due to a sudden increase in renewable energy output and a low market demand [4]. In some areas, negative electricity prices are further increased due to the fact that large generating facilities would rather sell at a loss to avoid decreasing their power level. This preference is caused by the high capital cost and relatively

low variable costs of large generating facilities [5].

Nuclear stations are typically one of these large generating facilities. As a result of the large construction costs and the fixed number of staff members that must be on site at all times, most utilities prefer to keep a reactor at full power, as it is easiest to maintain constant power. If instead of remaining at full power, a nuclear station operated in load-following mode, could this increase the efficiency of the plant? During load-follow operation, a nuclear station will vary its power output in response to the anticipated demand to better suit the market needs, stabilizing the price of electricity. Theoretically, the currently operating plants were all designed with the maneuverability to respond to such change in demand [6]. In fact, many of the reactors in France already participate in load-following maneuvers with the help of grey control rods [6]. Grey control rods are similar to standard Pressurized Water Reactor (PWR) control rods but have significantly less rod worth [7]. The low rod worth allows them to be used for reactivity control without putting significant stress on the surrounding fuel. In the U.S., grey rods are not present in PWR, increasing the complexity of load-follow operation [6].

Previously load follow demonstrations have been performed in U.S. PWRs. In the 1970's Indian Point underwent a series of load-follow power maneuvers, where 50 % power swings performed using ramp rates that varied between 0.25 and 5.0 % power/minute [8]. The primary purpose of this study was to demonstrate the plants ability to maintain control over the AO during/following the power maneuvers. If control over the AO is lost, control rods may not have the strength to effect the core power distribution in the presence of local xenon concentrations [8]. With insufficient control over the flux profile local linear heat rates could exceed safety margins.

In order to mitigate this possibility, PWR use the critical boron concentration to modify the power level while making minor control rod insertion and inlet temperature modifications to manage the core AO [9]. Although it is ensured that safety margins are maintained, the insertion of control rods, in addition to the response of the local Xenon concentrations, can lead to significant changes in local pin powers throughout the core. Changes in local power can cause fuel to swell or contract, due to thermal expansion [10]. If a utility chooses to ramp down the reactor during times of low demand, or high supply, the fuel pellets will contract. When the decision is made to return the reactor back to full power, the rate at which the power can be increased is limited by the thermal expansion of

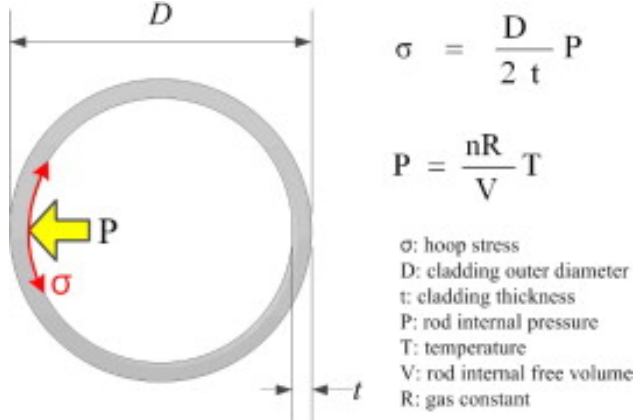


Figure 1.1: Visualization of the hoop stress acting on the fuel cladding using the thin wall approximation [1]

the fuel pellets [10]. A sudden expansion of the fuel pellet has the potential to exert additional stress on the cladding, commonly referred to as Pellet-Cladding Material Interaction (PCMI). PCMI can lead to fuel failure by Pellet-Cladding Interaction (PCI), and has been extensively investigated since the early 1970s.

### 1.1.1 Pellet Clad Interaction

PCI induced fuel failure is the result of PCMI and environmental contributions. PCMI is best described as the material interaction at the pellet-clad interface which creates a stress state on the fuel cladding [11]. This stress state is normally quantified using the maximum cladding hoop stress, which occurs at the inner radius of the cladding. In a cylindrical fuel rod hoop stress, shown in Figure 1.1, is a function of the pressure being exerted on the cladding through fuel pellet contact and the pressure difference between the gap and coolant.

To determine the magnitude of the cladding hoop stress the shape of the fuel pellets must be accurately known. The shape of the fuel pellets controls the volume of plenum, influencing the gap pressure, and in the case that the gap has closed, the fuel pellets shapes are restrained by the cladding. Many different factors contribute to the shape of the fuel pellet, including temperature of the fuel, fission product inventory, power history and manufacturing characteristics. During power maneuvers, the fuel temperatures are the most significant as it determines the degree to which the fuel expands. To further complicate the geometry of the fuel pellet, uneven thermal expansion

during the initial ramp to power causes radial cracks to form within a pellet [12]. These cracks, in addition with thermal expansion, lead to shear forces and hoop stress on the inner radius of the fuel cladding.

In addition to the mechanical stress being exerted on the cladding, environmental contributions, chemical or geometrical in nature, have an adverse effect on the claddings integrity. Chemical environments arise from the release of fission products from the fuel pellet. Iodine and cadmium-in-cesium are considered to be the most corrosive fission products released from the pellet [12]. In the presence of prolonged PCMI, the corrosive chemical environment causes inter granular crack propagation, or Stress Corrosion Cracking (SCC), through the zircaloy based cladding. This type of cladding failure is commonly referred to as PCI-SCC, or "classical PCI."

Geometric contributions to PCI are a result of irregularities in the fuel pellet shape. Typical Light Water Reactor (LWR) fuel pellets are ceramic  $UO_2$  cylinder with a height of approximately 1 cm and dishes and chamfers on the top and bottom of the pellet. Hundreds of these pellets are stacked into a single fuel, with approximately 60,000 fuel rods in a LWR core. The sheer quantity of fuel pellets ordered by a utility makes it impossible for a fuel vendor to ensure no pellet has a defect. The most common defect is a Missing Pellet Surface (MPS), where part of the fuel pellet has chipped off during manufacturing. This chip causes asymmetric expansion of the pellet during power maneuvers leading to an increased local stress on the fuel cladding [12]. If this stress exceeds the yield stress of the cladding, brittle failure is likely to occur. This type of cladding failure is commonly referred to as PCI-MPS, as the missing surface is the critical feature in causing the failure.

## 1.2 Literature Review

In the early 1970's a string of fuel failures in Boiling Water Reactor (BWR) led to the first classification of PCI induced fuel failure. Shortly after, PCI induced fuel failures were found in PWR and determined to be an inherent problem in LWR zircaloy based fuels. The majority of these failures were observed during or shortly after power maneuvers from hot zero power. To reduce the risk of failure, fuel manufactures made design modifications and began to provide power ramping guidelines [11]. These ramp guideline were particularly conservative and focused primarily on BOC

power ramps. Since then, PCI has been extensively studied in order to increase the efficiency of reactor start-up and minimize the number of fuel failures.

Cox [13] performed an extensive review of the work done on zircaloy fuel failures caused by PCI up to 1972. He found that fuel pellet geometry is the most significant factor in PCI. The strain on the cladding is determined by

1. manufactured gap size
2. shape of the fuel pellet
3. effect of the chamfers and grooves.

In addition to manufactured defects in the fuel pellets, ceramic  $UO_2$  fuel pellets also experiences a number of geometric changes as a function of radiation exposure and temperature/power level. These changes include, but are not limited to, fuel pellet densification, cracking, relocation, and thermal expansion. Pellet cracking and relocation contribute significantly to the strain experienced by the cladding due to the differential movement of the pellets relative to one another. This differential movement is further intensified by the locking of crack edges into cracks within the cladding and the local coefficient of friction between the pellet/cladding. At high exposure the coefficient of friction can approach infinity as fission products have escaped the fuel pellet and cemented the pellet to the cladding, leading to intensified stresses during power maneuvers.

In addition to the contribution the fuel pellet geometry has on the local strain, the cladding material and geometry determine how the cladding will respond to the strain. The wall thickness to diameter ratio and creep rate of the cladding effect the magnitude of the initial stress and the rate at which the stress decays. The total stress imposed on the cladding is a function of the maximum power, which determines the total expansion of the fuel pellet, and the change in power during a power ramp, which determines the increment in cladding strain. Cox goes on to highlight the importance of a corrosive agent at causing PCI, noting that Iodine and Cadmium-in-Cesium are the largest contributors to the corrosive environment at the cladding surface. To minimize the risk of PCI, Cox emphasized the importance of fuel conditioning and holds at intermediate power during large power ramps.

The term fuel conditioning is commonly used by researchers and industry representatives when

discussing power maneuvers, yet the quantitative definition of conditioning can be difficult to find. Capps et al. describes fuel condition as the state of the fuel rod when considering the changes in the fuel, cladding and gap [12]. Many of these changes are a result of the pellet and cladding's response to radiation and heat transfer, for example

- fuel pellet cracking and relocation are caused by the thermal expansion of  $UO_2$ ,
- fuel pellet densification is caused by radiation exposure,
- fuel pellet swelling is caused by fission product accumulation,
- grain growth in fuel pellets is caused by elevated temperatures,
- and creep deformation in the pellet and the cladding occur due to elevated temperatures and radiation exposure.

Due to the fact that all of these changes are dependent on the local power and exposure, a concrete definition of fuel conditioning is difficult to create. Rather, fuel conditioning describes the ability of the fuel rod to respond to rapid changes in power [12]. During conditioning the cladding is able to relieve some of the stress experienced during a power increase while also influencing the chemical environment at the surface of the pellet [13]. Together these effects reduce the propagation of cracks, limiting the possibility of PCI induced fuel failure.

Jernkvist [14] developed a model for predicting PCI induced fuel failure based on crack initiation and growth. Jernkvist model stressed three key parameters involved in PCI,

- cladding stress and strain are extremely localized,
- fuel rod failure due to PCI is normally a result of a sudden power increase
- PCI induced failure within a reactor core shows strong variability.

Due to the presence of internal flaws within the cladding, Jernkvist neglected the intergranular process and only considered transgranular crack growth. In order to account for the stochastic nature of PCI in reactor cores, a probabilistic treatment of the initial crack size was used. The crack propagation velocity was then determined by the stress, temperature, and iodine concentration at the tip of the crack. Using a finite element solver, Jernkvist calculated the stress at the tip of the

crack. If the stress was greater than the iodine stress corrosion crack threshold, the velocity was determined using a correlation requiring the temperature and iodine concentration. To simplify the determination of the iodine concentration, a correlation was used based on the power and fuel burnup. It was then assumed that all of the iodine collects at the pellet-pellet interface and radial pellet cracks.

With the velocity of the crack propagation known the time to cladding failure can be calculated. Using an artificial power history, Jernkvist provides an example where the coefficient of friction is varied for the pellet-clad interface. At sufficiently high coefficients of friction, the local stress on the cladding is high enough to grow the crack through the cladding. This demonstration shows the importance of accurately determining the stress within the cladding when trying to predict cladding failure. Additionally, it highlights the need for a coupled multiphysics approach as the coefficient of friction at the pellet-clad interface is a function of temperature and burnup.

One of the computational codes that attempts to incorporate this multiphysics approach is FALCON [15]. FALCON is a fully coupled, thermo-mechanical, two dimensional finite element computer code being developed by ANATECH. Building on the material properties provided in MATPRO, FALCON has the ability to simulate  $UO_2$  pellet relocation, fission gas release and zircaloy cladding thermal creep.

FALCON has been extensively benchmarked and is commonly used by contractors and utilities to mitigate the risk of PCI induced fuel failure. Lyon et al. [2] used FALCON in order to determine a criteria for mitigating PCI induced fuel failure during power ramps. The authors point out that power ramp rate restrictions, which are normally set by fuel vendors, and fuel conditioning are not reliable at mitigating the risk of PCI. Rather, these practices lead to restrictive constraints on plant operation.

Another criteria that is commonly suggested by fuel vendors is the implementation of a stress based threshold. Unfortunately, stress based thresholds are typically unable to distinguish between failed and non failed fuel rods, leading to a conservative threshold when applied to power maneuvers [2]. Lyon et al, proposes a mechanistic approach that incorporates PCMI and SCC based cumulative damage.

Similar to Jernkavist, Lyon et al. recognized that cladding failure due to SCC occurs in two

stages, crack incubation and crack propagation. The Cumulative Damage Index (CDI) model in FALCON accounts for both of these stages using a cumulative damage process, where damage accumulation is linear with time. This allows the damage fraction,  $D$ , to be defined as

$$D = \int \frac{dt}{\bar{t}} \quad (1.1)$$

where  $\bar{t}$  is the time-to-failure. The time-to-failure of a material is normally measured in an SCC out-of-pile test and is defined as

$$\bar{t} = f(\sigma, \sigma_y, \sigma_{ref}, B, T) \quad (1.2)$$

where  $\sigma$  is the applied hoop stress,  $\sigma_y$  is the materials yield strength,  $\sigma_{ref}$  is burnup dependent function,  $B$  is the burnup of the fuel, and  $T$  is the temperature. It is important to note that Equation 1.1 only applies to a single power maneuver, therefore  $D$  must be summed over all power maneuvers. Experience has shown that  $D$  exhibits logarithmic behavior with stress, therefore it should be interpreted probabilistically, where  $D = 1$  represents a 50% failure probability while  $D = 0.1$  and  $D = 10$  imply a  $< 5\%$  and  $> 59\%$  failure probability. In order to account for the possibility that cladding stress can drop below the SCC threshold during ramps and environmental difference between in-pile and out-of-pile fuel rods, an adjustable single valued parameter  $\beta$  is introduced to the CDI model.

$$D = \sum \frac{\delta t_i}{\beta \bar{t}_i} \quad (1.3)$$

In order to demonstrate the accuracy of a CDI based criteria, Lyon et al. simulated 14 fuel rods from the Studsvik Over Ramp, Super Ramp and Trans Ramp IV program, as well as, rods from a CEA/OSIRIS ramp program using FALCON [16]. These simulations were broken into three parts, first a steady state two dimensional, R-Z, depletion simulation is performed using the power histories of each rod. The results of these simulations are then used as the initial condition for transient R-Z simulations of the different power ramps under investigation. Finally, an R- $\theta$  model containing discrete fuel cracks is created for the axial location which experienced the highest R-Z hoop stress. This simulation provides the fuel pins maximum clad hoop stress and CDI which can then be used to determine a threshold criteria.

After validating the steady state simulations against Post Irradiation Examination (PIE) mea-

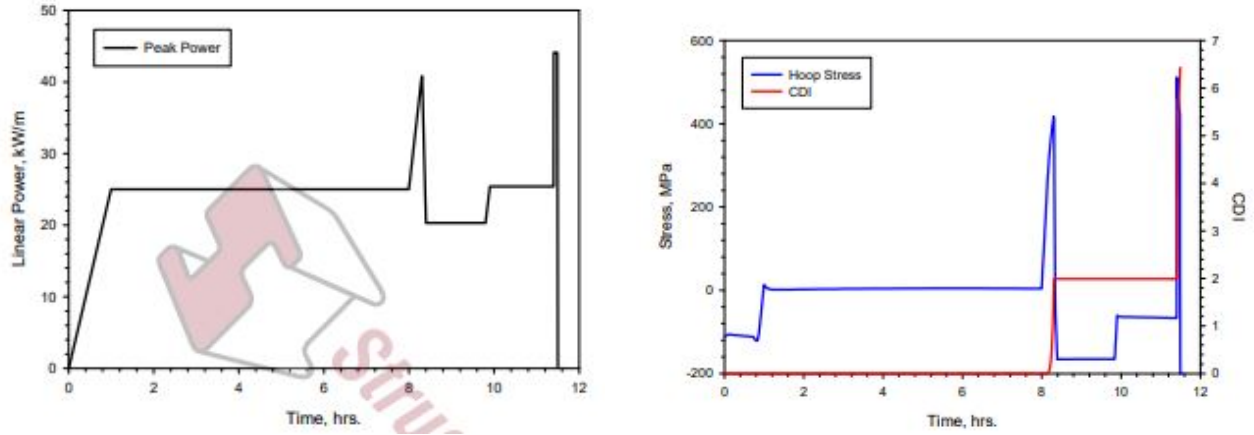


Figure 1.2: The Power history (left), Falcon predicted hoop stress and Falcon predicted CDI (right) for Q11/1 of the Studsvik ramp program [2]

surements, Lyon et al. performed the transient analysis for all of the fuel rods. The power history of fuel rod Q11/1, along with the maximum cladding hoop stress and CDI are shown in Figure 1.2. It is observed that the CDI only changes during sharp power ramps while the hoop stress more closely follows the power profile.

Using the results of all 14 fuel rods, the authors established a statistical failure criteria using both hoop stress and CDI. A 550 MPa maximum clad hoop stress and a CDI of 5.85 were determined to signify a 50% chance of rod failure. Using the 50% chance as a hard cut off between non-failed and failed rods, the authors evaluated how each of the criteria performed using the 14 fuel rods. The peak stress was able to correctly predict the behavior of eight out of the 14 fuel rods while the CDI predicted the behavior of 13 out of the 14 rods. Although this work does show the superiority of a CDI based criteria, the training set and validation set are considerably small. Additionally, the power ramps used during the test program are extreme and are unlikely to be performed during standard operation or load-follow operation. As a result, further validation is needed before deciding if a CDI based criteria is reliable.

Similar to Lyon et al., Capps et al. [17] used BISON to investigate fuel rods that failed during the start up ramp of a commercial PWR. Before Capps et al. could begin applying failure thresholds to fuel rods under investigation, the thresholds needed to be determined using BISON as the thresholds are specific to the performance code. To do so, the Studsvik ramp tests were implemented in BISON using a four step process [16]. The first three steps follow the same methodology used by Lyon et al,

R-Z depletion followed by an R-Z fuel performance calculation, ending with a R- $\theta$  fuel performance calculation at the axial location with the highest hoop stress. The fourth step, which is unique to BISON, is a three dimensional R- $\theta$ -Z fuel performance simulation of the entire rod. Although BISON is capable of computing CDI, the authors only report the failure thresholds based on the peak cladding hoop stress. The results of both the R- $\theta$  and the three dimensional simulations were consistent with the results presented by Lyon et al. The authors observed that the hoop stress calculated in the three dimensional study was consistently higher than the hoop stress from the R- $\theta$  study. This signifies the importance the pellet's height has on the cladding stress. Although the three dimensional stress was elevated no clear cutoff was observed to distinguish the failed fuel rods from the intact fuel rods. For this reason, a statistical approach was developed for both the R- $\theta$  and the three dimensional simulations.

Using the same four step methodology, the authors performed fuel performance simulations on several fuel rods from the commercial PWR. Two different cycle startup ramps were investigated; the first cycle contained three failed fuel rods and the second contained a single failed fuel rod. The power histories for the R-Z depletion were provided by Westinghouse and are assumed to be from a nodal core simulator. Before analyzing any of the BISON results the authors observed important characteristics from the fuel rods power histories. Two of the failed rods in the first cycle were exposed to aggressive linear heat rates during their initial cycle. This led to the rods accumulating high burnups and the closing of the gap. The third failed rod saw a significant increase in its linear heat rate after its initial cycle. As noted in the previous works, these characteristics are strong indicators each rods conditioning.

In order to account for the change in cladding material, zirc4 in the Studsvik tests, zirlo in the commercial reactor, Capps et al. scaled the 5% failure thresholds to 395 MPa for the R- $\theta$  and 446 MPa for the three dimensional predictions. The peak cladding hoop stress for all three of the failed rods was predicted to be below the threshold in both simulations. Additionally, two of the non-failed rods that were predicted to have peak cladding hoop stress above the threshold. This led the authors to conclude that "classical" PCI could not be the cause of the failure. After introducing a MPS to each of the simulated rods, all peak cladding hoop stresses fell above the 5% failure threshold. Furthermore, one of the fuel rods was confirmed to have a MPS during a PIE,

confirming the predictions of the simulation.

In order to reduce the probability of PCI induced failure, classic and MPS induced, Exelon implemented strict power ramp rates and began to introduce power holds during return to full power ramps [17]. Capps et al. investigated the effects of these restrictions on the cladding hoop stress and found that they could reduce the peak stress by approximately 50 MPa. Even with this reduction in failure risk, fuel failure was still experienced during the initial power maneuver. This suggests that pellet defects are a major contributor to fuel failure during power maneuvers. Using the restrictive power history developed by Exelon, Capps et al. performed a sensitivity study on the maximum clad hoop stress as a function of MPS width.

Fuel specifications limit the dimension of a MPS to 60 mils, but widths up to 125 mils have been observed during PIE [18]. For this reason, MPS with lengths ranging from 60 to 140 mils were simulated using 2D and 3D BISON simulations. The hoop stress resulting from a MPS is a result of pellet thermal expansion. As the pellet expands the missing face does not exert an outward force on the cladding, causing the cladding to bend at the edges of the MPS. In 2D simulations the hoop stress increases linearly with the length of the MPS, with a widths of 110 mils increasing the probability of failure to 50%. These simulations are inherently flawed as adiabatic boundary conditions are applied to the top and bottom the fuel slice, resulting in the limitation that heat must be conducted radially. As the missing pellet surface grows, the heat transfer across the gap degrades leading to an increase in pellet temperature. This increase in temperature causes the pellet to continue to swell, exerting additional pressure on the cladding.

In reality, the heat will flow in the direction of the least resistance, i.e. axial conduction will compensate for the reduction in heat transfer across the gap. This effect is captured in the 3D simulations, which show minuscule changes in the maximum fuel temperature as a function of MPS width. A MPS width of 100 mils was found to result in a 50% chance of fuel failure during the restrictive power ramps. Unfortunately, the 3D simulations were performed using an infinite coefficient of friction between the pellet and cladding, causing elevated stresses in the cladding when compared to the 2D simulations. This prevents a meaningful comparison on the effect fuel temperature has on the failure thresholds in 2D and 3D simulations.

In order to more comprehensively understand the effect pellet defects have on the cladding,

Capps et al. studied the individual effects of fuel cracks and MPS [12]. The stress on the cladding caused by pellet cracks is a function of the crack length and the spacing in between cracks. As the crack spacing increases within the fuel pellet the number of cracks within the pellet decreases. This causes the opening of a single pellet to increase, which increases the tangential stress on the cladding at the cracks opening. It is typically found that commercial fuel has six to ten radial cracks, which helps to reduce the stress on the cladding [19].

The length of a fuel pellet crack characterizes the compliance of the fuel pellet to its manufactured cylindrical shape. As the crack length increases, the fuel pellet is less compliant and creates a shear stress on the cladding. Capps et al. found that the shear stress exerted begins to saturate when the crack length approaches 50% of the pellet radius. Although the stress on the cladding has saturated, the stress at the tip of the crack is larger than the fracture strength. This suggests that the crack will continue to propagate until it has reached approximately 70% of the pellet radius.

In most cases, MPS are accompanied by cracks. This makes it necessary to incorporate pellet cracks when determining the effect of MPS. Unlike pellet cracks, MPS cause hoop stresses within the clad through bending forces. This hoop stress shows a saturation as the MPS width increases. In addition to the width of the MPS, the shape of the defect has a strong effect the maximum hoop stress. It is typical to simulate MPS as flat defects, although it is more likely they will be concave in shape. This concavity further reduces the pellet-gap conductivity causing a rise in the fuel temperature and an increase in the maximum hoop stress.

Although 2D simulations are useful in determining the effect of fuel cracks and MPS, they are inherently flawed as much of the axial effects are lost in the boundary conditions. In addition to the loss of heat transfer in the axial direction, structural support is not taken into consideration as the MPS has an infinite height. Unfortunately three dimensional contact makes the simulation of cracks and MPS difficult, and prohibits a full length fuel rod from being simulated in three dimension. To work around this, Capps et al. simulated a stack of five discrete fuel pellets with a MPS included in the center fuel pellet. The results of the three dimensional study showed that axial contributions reduce the maximum cladding hoop stress by 7 to 15 %. Although this reduction is significant, the trends observed in the two dimensional studies did not change. Therefore, fuel performance studies can be conducted in two dimensions as long as the thresholds for stress were determined

using consistent two dimensional studies.

Knowing the statistical thresholds and the importance of cladding defects in regards to fuel failure, analysts can determine the risk of fuel failure for a given core power maneuver. Typically the initial ramp to full power is given the most attention but in the case of load-load follow operation all power maneuver will need to be analyzed to determine the risk of fuel failure. Unfortunately, it is far to computationally expensive to perform a PCI focused fuel performance simulation for all of the rods within the core for each of the ramps under consideration. In order to reduce the number of simulations required most utilities or contractors will focus on a small number of assemblies within the core. Kennard et al. describes how to go about reducing the 193 fuel assemblies found in a commercial PWR down to about 6 assemblies [11]. The screening process looks to see if 1) an assembly has seen a significant power increase since its previous cycle, 2) exposure falls above a critical value, and 3) the ratio of the maximum power to the conditioned power is large. Typically a core simulator will provide the predicted pin powers, which are needed to screen the power maneuver. The assemblies selected are then considered the limiting assemblies for the power maneuver and are analyzed using a fuel performance simulator. Kennard et al. applied this screening process to a commercial PWR start up ramp. The pins within the limiting fuel assemblies were analyzed using FALCON and the methodology presented by Lyon et al. [2].

Based on the 1% failure threshold for a FALCON fuel performance simulation, Kennard et al. make recommendations to mitigate the risk of PCI induced fuel failures for a number of generic operating conditions. Two recommendations are made in regards to load-follow operation, the first being the importance of maintaining AO control. During a return to full power maneuver, the local xenon concentrations and moderator temperature coefficient will cause the core AO to swing. If the AO swing is significant enough local power levels may exceed conditioned power levels causing a sudden expansion of the fuel pellet. Strong control over the AO will reduce this risk, mitigating the chance of fuel failure. The second recommendation is better described as a warning. Kennard et al. warn that local power uncertainties can increase the stress experienced during returns to full power after a reduced power hold. This recommendation highlights the importance of accurately knowing local power at the pin cell level. Many core simulators would use a nodal core simulator and pin power reconstruction to calculate the pin power as a function of time. This reconstruction

is likely to introduce uncertainty in the pin powers leading to uncertainty in the fuel performance results.

In this work, VERA Core Simulator (VERA-CS) is used to simulate load-follow operation of a commercial PWR. VERA-CS is capable of accurately predicting pin powers allowing for reduced uncertainty in fuel performance results. In addition to the reduced uncertainty in fuel performance results, the fidelity of the VERA-CS results allow for a pin focused screening process in place of an assembly based process. By focusing on individual pins the number of necessary fuel performance calculations can be reduced allowing for the examination of more severe load-follow maneuvers. In the remaining chapters the results of load-follow focused fuel performance calculations will be presented for the operating history of a commercial PWR. In Chapter two the preliminary work required to perform fuel performance calculations will be presented, including a description of the PWR1 model and the VERA-CS code. A detailed description of the BISON fuel performance code and the pin based screening process are presented in Chapter 3. In Chapter 4 the results of the fuel performance calculation will be analyzed using the pin based screening process. In closing, the conclusions drawn from this work and possible future extensions will be contained in Chapter 5.

# Chapter 2

## PWR1

University of Illinois at Urbana-Champaign (UIUC) partnered with Consortium for Advanced Simulation of Light Water Reactors (CASL) to investigate load-follow operations in a PWR. The objective of the work was to investigate the effects of load-follow operation specific to an operating PWR. At request of the owner, the reactor chosen was not be disclosed, but it will be referred to as PWR1. PWR1 was chosen due to the significant load follow maneuvers that occurred during operating cycle 21. To provide an accurate power history and isotopic composition for the load follow operation during cycle 21, it was decided that a jump-in depletion would be performed starting four cycles earlier, i.e. cycle 17. This decision is due to core loading patterns that include assemblies shuffled from two cycles prior (e.g. cycle 21 includes assemblies introduced in cycle 19, whereas cycle 19 includes assemblies introduced in cycle 17). By the advice of CASL, it was determined that any approximations of power histories or isotopic compositions introduced to the model in cycle 17 would have a negligible effect on the results obtained in cycle 21.

### 2.1 PWR 1 Model Description

PWR1 is a four-loop Westinghouse PWR. Each core loading has 193 Westinghouse 17x17 fuel assemblies, comprised of 264 fuel rods, 24 guide tubes and one instrumentation tube. Each fuel rod consists of two axial regions, a blanket and a mid-section. Within the mid-section, the enrichment of each rod is selected to ensure sufficiently low power peaking and a desired cycle length. The enrichment within the blanket is typically lower than the mid-section to reduce axial leakage from the core. In addition, a thin layer of zirconium diboride may be applied to the mid-section of a fuel pin. This thin coating, known as an Integral Fuel Burnable Absorber (IFBA), allows for greater reactivity control throughout the life of the fuel rod. One drawback of IFBA coating is an increase

in the plenum pressure as the absorber is burned. To compensate for this increase in pressure, annular pellets are used within the blanket region.

The VERA model includes the core plates, nozzles, gaps, two Inconel and six Zircaloy spacer grids, and three intermediate flow mixer (IFM) grids. In addition, a total of twenty-four different assembly designs were used in the various cycles of interest. All core and assembly geometry details necessary to model PWR1 in VERA-CS were collected and provided by the industry partner.

### 2.1.1 VERA-CS

CASL's primary computational tool suite, VERA-CS, incorporates coupled physics and science-based models, state-of-the-art numerical methods and modern computational science applied to reactor core simulation. VERA-CS achieves this task by integrating three well-developed physics simulators with other supporting sub-components. In the present work, we used the deterministic neutronics solver, MPACT, coupled with the sub-channel thermal-hydraulics solver, CTF, to perform detailed simulations down to single-pin resolution, as shown in Figure 2.1. The fuel performance (thermo-mechanical) code, BISON, was used to construct fuel temperature tables, which related the temperature of the fuel to the temperature of the cladding as a function of burnup and linear heat rate. A significant advantage of the VERA-CS system is the reduction of overall modeling effort by unifying all solver components into a single user-friendly input specification (called VERAin) and a single binary output file. The VERAin input file is an ASCII text input based on geometric and material descriptions that is parsed out to each code (physics) component through built-in tools. Below is a brief description of two of the primary simulators that are part of the VERA-CS system used for this work, the BISON fuel performance simulator will be presented in Chapter 3.

## MPACT

MPACT is a neutron transport solver being developed by the University of Michigan (UMich) and Oak Ridge National Laboratory (ORNL). It provides pin-resolved flux and power distributions [20]. To solve three-dimensional (3D) problems, it employs a 2D/1D method, which decomposes the problem into a 1D axial stack of 2D radial planes [21]. These planes are then solved using

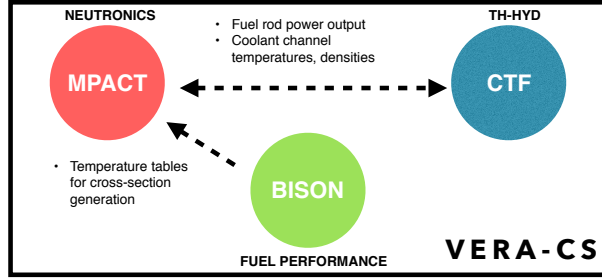


Figure 2.1: Primary physics simulator components of VERA-CS used in this work.

Method of Characteristics (MOC). While there are a variety of axial solvers available, the Nodal Expansion Method (NEM)-simplified P3 (SP3) solver is the default, which wraps a one-node NEM kernel [22]. These 2D and 1D solvers are coupled together through transverse leakage to ensure neutron conservation, and they are accelerated using 3D Coarse Mesh Finite Difference (CMFD).

## CTF

CTF is a subchannel TH code being developed by ORNL and North Carolina State University (NCSU) for LWR analysis [23]. It simulates two-phase flow with a three-field representation (liquid, droplet, and vapor) assuming the liquid and droplet fields are in a dynamic equilibrium, leaving two energy conservation equations. CTF provides significantly higher resolution and physical detail than the internal TH solver in MPACT, thus requires longer execution times.

### 2.1.2 Work Flow and Modeling Strategy

Several steps were involved in producing an accurate neutronic/thermal-hydraulics core model. Figure 2.2 displays the VERA-CS modeling stages used in this work.

In most cases, each cycle includes assemblies from the previous two cycles, which necessitates a total of five cycles of depletion simulation to provide an accurate isotopic composition and power histories for the oldest assemblies present in cycle 21 (from cycle 19). Although it would be most accurate to start modeling from the Beginning of Life (BOL) of PWR1, this is computationally impractical. In this work, individual pre-burned assemblies were inserted into the cycle 17 core model through a "jump-in" strategy to approximate the shuffled assemblies present in cycle 17

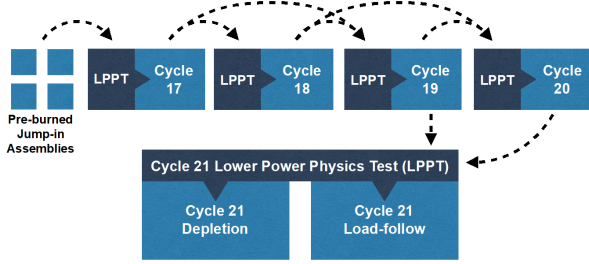


Figure 2.2: Modeling strategy to simulate load follow in PWR1 cycle 21.

(from cycle 15 and 16). These approximate assemblies are removed from the core by the start of cycle 19, which minimizes their effect on isotropic accuracy of our target cycle, cycle 21.

Because of the difficulties in performing single assembly 3D depletion, special attention was paid to the exposure axial offset of each assembly at its desired burnup. During the project it was determined that the exposure axial offset needs to be close to zero to prevent an unrealistic power axial offset from occurring in cycle 17. In order to approximate cycle 15 and 16 assemblies as closely as possible, a total of 7 assembly types were burned to 15 target burnups. These 15 assemblies were then inserted into the proper position in cycle 17, based on the core loading scheme.

## 2.2 VERA-CS Results

### 2.2.1 Low Power Physics Testing

Before the cycle depletion was simulated, a Low Power Physics Tests (LPPT) was conducted to validate the shuffling scheme for each cycle, as shown in Figure 2.2. The LPPTs included a critical boron search, an Isothermal Temperature Coefficient (ITC) test and a Control Rod Worth (CRW) test. The ITC test was conducted by varying the temperature of the fuel and moderator by  $\pm 4$  °F. The change in reactivity was then used to determine the ITC. The CRW tests were performed using a Dynamic Rod Worth Measurement (DRWM) technique, where each control rod bank was individually inserted into the core and the change in reactivity was used to determine the control bank's worth. The comparison of the calculated critical boron, ITC and CRW to their measured value is shown in Table 2.1, and Figure 2.3, respectively. It is observed that the MPACT accurately

Table 2.1: Low Power Physics Results

Cycle	Critical Boron Difference [ppm]	Isothermal Temp. Coeff. Difference [pcm/ $^{\circ}$ F]
17	-42	-0.6
18	44	-1.4
19	1	-1.7
20	3	-0.83
21	-10	0.4

predicts the measured critical boron value from cycle 19 onward. The ITC predictions are within 2 pcm for all cycles, which is within a reasonable margin of error. In addition, it is observed that the predicted CRW values are all within  $\pm 6\%$ . It is observed that from cycle 19 onward, the CRW values for the different control banks tend to become more irregular. Regardless, the total predicted control rod worth was within 1 % for cycle 19, 20 and 21, which is within measurement uncertainties. It should be noted that some of the large relative errors observed in the control rod worth comparisons are a results of low measured rod worth. Based on these comparisons, it is concluded that any error introduced by the individually burned assemblies inserted into cycle 17 is eliminated by cycle 19, which shows an excellent agreement with the measured values.

### 2.2.2 Cycle Depletion

After the shuffling scheme for each cycle had been validated, cycle depletion was simulated from the BOC to the EOC, with special attention paid to the shutdown time between EOC and BOC of the next cycle to ensure accurate fission product decay between cycles. As the fuel is depleted over a reactor cycle, the boron concentration in the coolant is reduced via dilution to maintain criticality. In addition to the boron concentration being diluted over the length of the cycle, the weight percent of  $^{10}\text{B}$  is also reduced. This reduction is a result of boron depletion and is known to increase the critical boron concentration during the later dates of the cycle. MPACT can account for boron depletion through explicit input of  $^{10}\text{B}$  enrichment, but this requires measurements of the  $^{10}\text{B}$  concentration before the simulation can be performed. As an alternative, the simulations is conducted with a constant  $^{10}\text{B}$  enrichment of 19.9 w/o and the measured critical boron is corrected using the measured  $^{10}\text{B}$  enrichment.

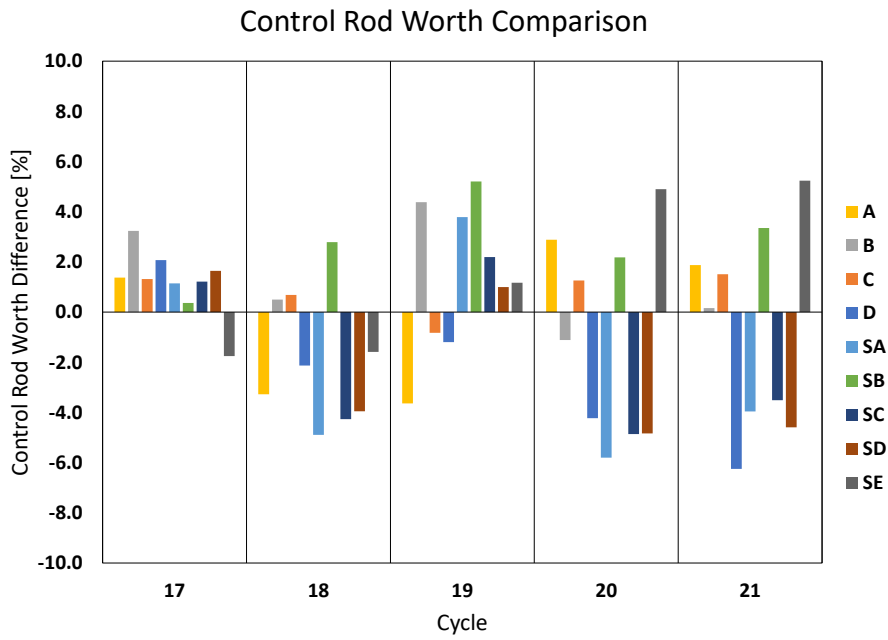


Figure 2.3: Comparison of control rod worth of all 9 rod banks at HZP.

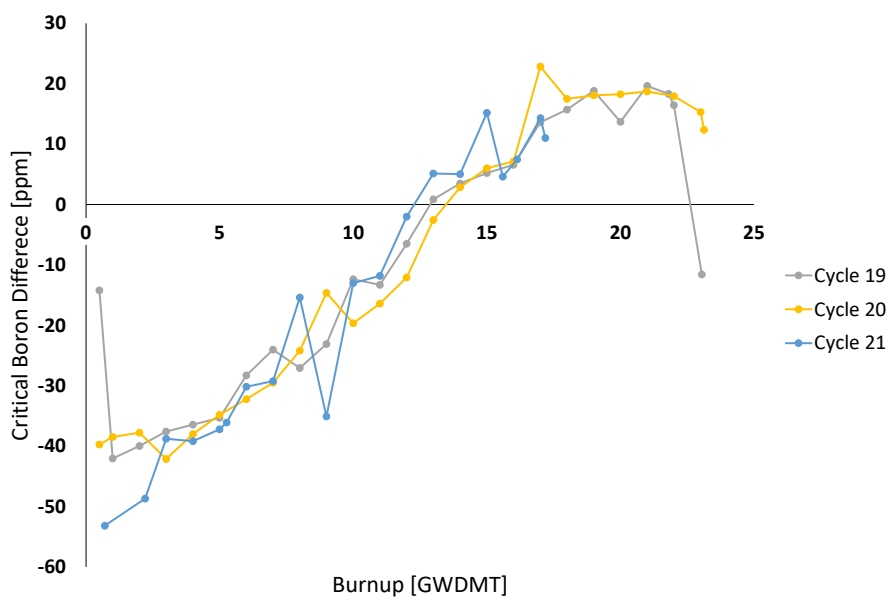


Figure 2.4: Comparison of simulated to the measured critical boron concentrations.

The measured boron concentrations were used to establish the accuracy of the core reactivity vs. fuel burnup. The boron "letdown" is compared for cycles 19-21 in Figure 2.4. Figure 2.4 contains a comparison of the corrected measured boron concentration with the MPACT simulation. As shown in Figure 2.4, the difference between corrected measured and simulated critical boron concentration varies between -40 ppm at the beginning of cycle to +20 ppm at the end of the cycle. The cause of this reactivity swing is believed to be the temperature tables used to determine the fuel's temperature as a function of burnup and linear heat rate. These tables are not used during Hot Zero Power (HZP) calculations, which show good agreement to the measured values, and are constant for all three cycles, which have very consistent discrepancies. Regardless, the difference is within 50 ppm for each cycle depletion, which is considered sufficiently accurate.

## 2.3 Load-Follow Operation

After further review of the test stand's depletion results, it was determined that the UIUC model of PWR1 displayed sufficient agreement with plant measured data. In addition to cycle depletion, hourly depletion simulations were performed for the first month of plant operation. During this time period, a total of 24 power maneuvers were performed, varying the plants power output between 100 % and 70 %. During the VERA-CS simulations the exact reactor power, control rod position, and moderator inlet temperature were modeled using hourly depletion steps. A graphical representation of the power histories, along with the predicted AO, can be found in Figure ??.

In order to validate the MPACT simulation, the critical boron was calculated during the load-follow simulation. The MPACT predicted critical boron and AO was then compared to the estimated critical boron and AO provided by the industry partner. Unfortunately, the estimated critical boron was obtained using the core monitoring system, which was shown to have incorrect critical boron concentrations before a kbias was applied. As a result, a direct comparison of the critical boron was not performed, instead a comparison of the critical boron response immediately following a kbias was used to validate the prediction. It is observed in Figure ?? that the MPACT predict boron response shows excellent agreement with the core monitoring system boron response during the load-follow power maneuvers at BOC. The comparison of the MPACT predict AO and the plant estimated AO allow for several conclusions to be drawn about the MPACT simulation.

At times when power is decreased, both the MPACT and plant AO are observed to increase. This behavior is expected as the moderator temperature coefficient should push power towards the top of the core as power is decreased. Unfortunately the MPACT predictions over estimate the magnitude of the positive swing. This overestimation could be a result of the temperature tables used in the simulation or could be a result of the under predicted control bank worth. Additionally, sinusoidal oscillations in the MPACT AO are observed during times of constant power following a power maneuver. These oscillations are not observed in the plant data but their magnitude is negligible as they are less than 1 % from peak to peak.

Further investigation is required to reduce the observed discrepancies. In general it can be concluded that the MPACT predictions are within plant measurement uncertainties. Therefore, the results of these simulations, linear heat rates and cladding surface temperatures, can be used as the boundary conditions in fuel performance conditions. The detailed pin level data that is available from the VERA-CS results allows for reduced uncertainties in the fuel performance boundary conditions leading to more accurate predictions of peak cladding hoop stresses within a pin.

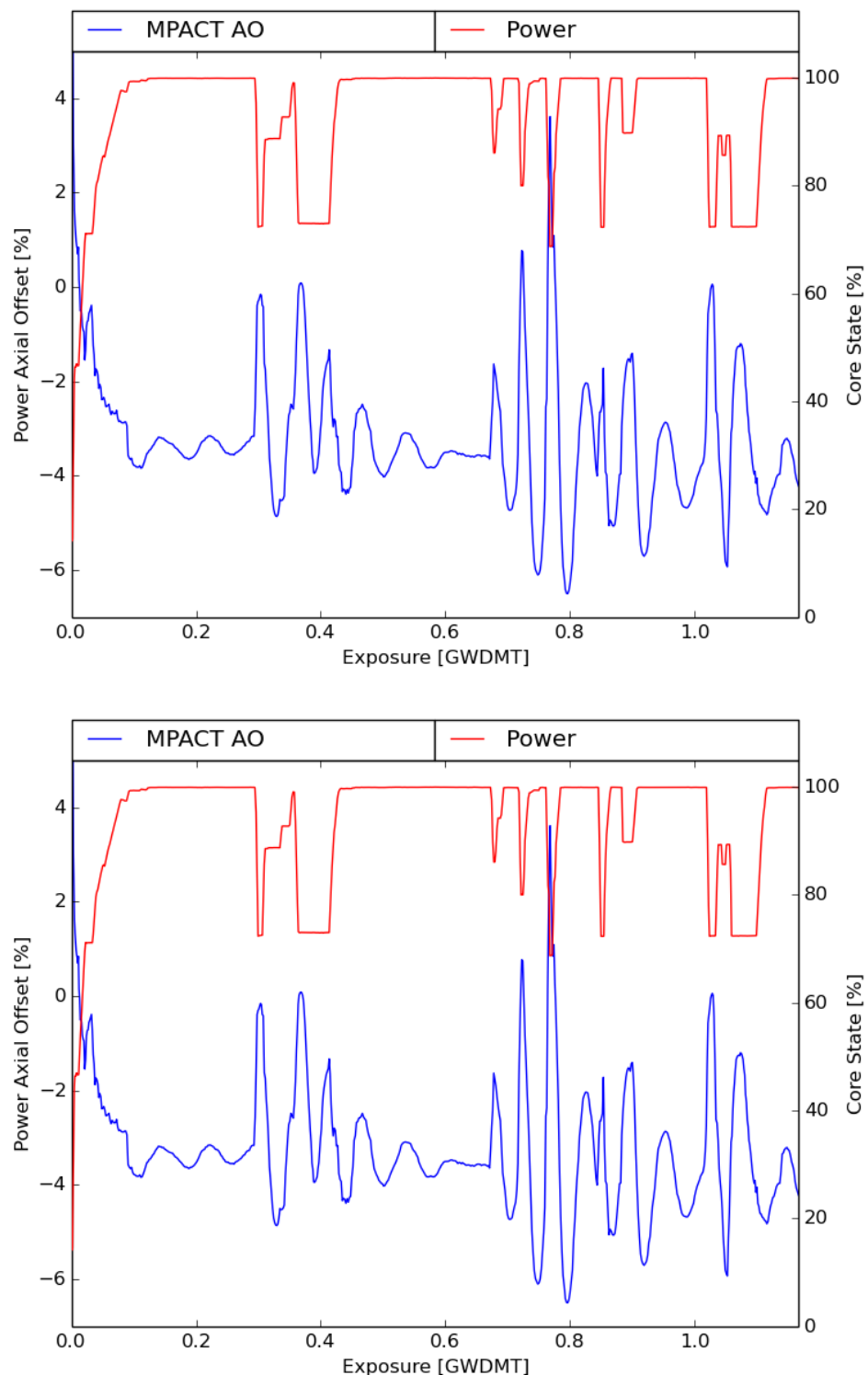


Figure 2.5: PWR1 hourly power history and predicted AO during the first 30 days of plant operation

# Chapter 3

## Methodology

The main focus of this work is to predict the limiting pin within a commercial PWR during load-follow power maneuvers. Due to the stochastic nature of PCI induced fuel failure and the randomness of pellet defects throughout the core, determining a single pin out of the approximately 60,000 present is unrealistic. Instead, it is desired that 1000 of the fuel pins be selected and analyzed using the three step process outlined by Lyon et al. [2]. Similar to the assembly based screening process developed by Kennard et al., the pin based screening process will look at characteristics indicating the fuels conditioning. In order to determine the validity of this screening process, all fuel pins contained within the quarter core VERA-CS model will simulated using the BISON fuel performance code. In the following sections the procedure for selecting the 1000 fuel pins and a description of the BISON fuel performance code will be presented.

### 3.1 MPACT Screening Process

As described in [12, 11], fuel rod response to a change in power is a function of the fuel rod's conditioning. In the presence of significant fuel exposure and/or operation at a high linear heat rate, the strongest indicator of elevated failure risk is a sudden increase above the conditioned power. To quantify the risk of PCI induced fuel failure, a weighted change in linear heat rate,  $R$ , is calculated for each fuel pin,

$$R_{i,j,k}^t = \frac{(lhr_{i,j,k}^t - lhr_{i,j,k}^{t_{con}})}{lhr_{i,j,k}^{t_{con}}} \cdot b_{i,j,k}^t \cdot lhr_{i,j,k}^t \quad (3.1)$$

where  $lhr$  and  $b$  are the MPACT predicted linear heat rate and burnup for fuel pin  $(i,j)$  at the axial location  $k$  and time  $t$ , respectively. For cycle start-up ramps, the conditioned power is taken as

the linear heat rate a shuffled fuel rod experienced at the end of the previous cycle,  $lhr_{i_{prev},j_{prev},k}^{t_{end}}$ . During a load-follow operation, the conditioned power is taken to be the linear heat rate experienced while operating at full power before the maneuver began,  $lhr_{i,j,k}^{t_{con}}$ . For example, in Figure 2.5 the linear heat rates calculated at hour 175 are assumed to be the conditioned linear heat rates for the following two power maneuvers,  $t_{con} = 150$ .

The weighted change in linear heat rate accounts for all parameters that effect PCI. The relative change from conditioned power determines if elevated stress are being applied on the claddings inner surface. Positive changes suggest that the fuel pellet has expanded, applying a tensile hoop stress on the cladding. Negative changes suggest that the fuel pellet has contracted, and fuel failure is unlikely. In the presence of a closed gap, the thermal expansion of the fuel pellet will cause elevated stresses on the cladding. Due to the fact that gap width is a complex function of power history, the fuels linear heat rate and burnup are used to determine the likelihood the gap has closed. When the fuel's burnup and linear heat rate are high it is unlikely that the gap is open. Additionally, the fuel's burnup suggests the presence of fission products on the clads inner surface. When multiplied, these three parameters indicated the fuel rods that are under elevated stress and have the potential to fail due to PCI.

An important parameter to consider is the effect prolonged load follow operation will have on the fuel's response. The degradation of the conditioned power, or the fuel deconditioning, is not well understood. The primary change in the fuel rod during deconditioning is a reduction of the cladding inner diameter. Cladding creep down, which is dependent on temperature, irradiation history, and applied stress, is the primary mechanism responsible for the reduction. For cycle start-up ramps, where the cladding and fuel rods are stored at reduced temperatures, deconditioning can be neglected. During extended periods of low power operation, where the cladding is exposed to elevated temperatures and stresses, it is possible that the cladding creep rate is not negligible. Therefore the conditioned power level could be a function of time spent at reduced power. A previous study [24] suggests that multiple power ramps have no effect on the conditioned power level of the fuel rod. However, the results presented by Stimpson [25] on continuous load-following for a single fuel pin suggest that changes in burnup have a strong effect on the maximum clad hoop stress. This effect is taken into consideration by the burnup factor in the weighted change in linear

heat rate.

## 3.2 BISON

The BISON fuel performance code is being developed by Idaho National Laboratory (INL) to provide single-rod fuel performance modeling capability to assess best-estimate values of design and safety criteria. BISON is built on INL's Multiphysics Object Oriented Simulation Environment (MOOSE) package [26], which uses the finite element method for geometric representation and a Jacobian Free Newton-Krylov (JFNK) scheme to solve systems of partial differential equations [27]. Three primary differential equations are implemented in BISON to determine the response of a nuclear fuel rod to changes in power. These equation describe the conservation of energy, momentum, and species, which are defined by,

$$\rho C_p \frac{\partial T}{\partial t} + \nabla \cdot \vec{q} - e_f \dot{F} = 0 \quad (3.2)$$

$$\nabla \cdot \vec{\sigma} + \rho \vec{f} = 0 \quad (3.3)$$

$$\frac{\partial C}{\partial t} + \nabla \cdot \vec{J} + \lambda C - S = 0. \quad (3.4)$$

$\rho$ ,  $C_p$  and  $T$  respectively describe the density, specific heat and temperature of a material subject to a volumetric heat source, described by  $e_f$ , the energy released per fission, and  $\dot{F}$  the volumetric fission rate.  $\sigma$  describes the Cauchy stress tensor under static equilibrium and a specific body force,  $\vec{f}$ .  $C$ ,  $\lambda$ , and  $S$  are the concentration, decay constant and volumetric source of a particular isotope. The implementation of these equations allows for non-linear kinematics and non-linear material behavior. This accounts for the temperature dependent thermal and mechanical properties of the nuclear fuel and incorporates the effects of material creep and plasticity. Further information on the implementation of material properties, including thermal conductivity, fuel swelling, creep and fission gas release, can be found in [28, 29].

In order to validate the predicted fuel response, a suite of experimental fuel rods have been simulated using BISON. Measured quantities including fuel centerline temperature, volume of gas released and pin diameter, are compared at BOL and End of Life (EOL) [28]. It is consistently

shown that BISON is capable of predicting fuel centerline temperatures within 10% of the measured value. Although a 10% error at elevated fuel temperatures,  $\pm 90$  °C at 900 °C, is significant, the measured linear heat rate of the experimental conditions is only accurate within 6%. This implies that a portion of the error can be contributed to measurement uncertainties, thus the 10% error is considered quite accurate. Fission gas release predictions are typically within a factor of two of the measured values. This agreement is considered within the range of measurement error and is common among many fuel performance simulators. Although fission gas release and fuel temperature show good agreement with measured quantities, rod diameter tends to be under predicted at BOL and over predicted at EOL. This discrepancy is believed to be caused by a lack of a relocation recovery model. Regardless, BISON has been shown to capture complex thermo-mechanical behavior such as PCI failures in PWRs [30, 17].

CASL has developed a methodology to perform fuel performance simulations for all fuel rods simulated using VERA-CS. The methodology relies on a template input file and a parser. Fuel performance calculations can be run coupled with VERA-CS, inline with VERA-CS or standalone. In this work fuel performance calculations are run standalone using a 1.5D template. This means that the linear heat rate and coolant temperature predicted using VERA-CS are applied as boundary conditions for the BISON calculations. Unlike an RZ simulation, the 1.5D template neglects axial conduction of the fuel rod. Rather, a stack of 1D pellets are coupled using a common plenum pressure. This geometric configuration has been shown to significantly reduce the computational time required for each power ramp [31]. Due to the fact that the RZ simulation commonly used for standalone BISON calculations uses a smeared pellet mesh, where individual pellets are not explicitly modeled, the 1.5D results are expected to have consistent predictions. In a standard PCI screening process, the results of RZ fuel performance simulation are used to select the axial location for a R- $\theta$  simulation. Therefore, with consistent boundary conditions between the RZ and 1.5D simulations, the reduced run time allows for additional fuel performance calculations to be conducted.

# Chapter 4

## Results and Discussion

Using the results of the load-follow and cycles depletion simulations, stand-alone bison inputs were created for all fuel pins contained within cycle 21. These inputs modeled each pins detailed power history, which accounted for core shuffling and cycle outages. An example of a shuffled pins power history is shown in Figure ??, where the pin was present towards the center core during cycles 19 and 20, and was then moved to the periphery of the core during cycle 21. Of the 14,784 found in the quarter core model of cycle 21, all but approximately 150 fuel pins ran to completion. After adjusting a radial biasing parameter within BISON, the 150 fuel pins ran to completion. This biasing parameter causes the fuel pin's simulated power output to exceed the specified input power. As a result, many of the parameters of interest, i.e. burnup, hoops stress, and gap thickness, may be overestimated. This behavior has been reported to the BISON developers and requires further investigation. Nonetheless, the maximum clad hoop stress within these pins is similar to the surrounding fuel pins, allowing the screening process to be applicable.

In the remaining sections the BISON fuel performance and MPACT screening results for the first 24 of operation are presented. The BISON fuel performance results are broken into four sections, the initial power ramp, and the first, second and third period of load-follow operation. The MPACT screening results follow the same format but the initial power ramp is not considered. Core designers spend a significant amount of time looking at the initial power ramp, therefor it is assumed a well accepted screening process has already been developed for the initial ramp.

### 4.1 BISON

#### 4.1.1 Start-up Power Ramp

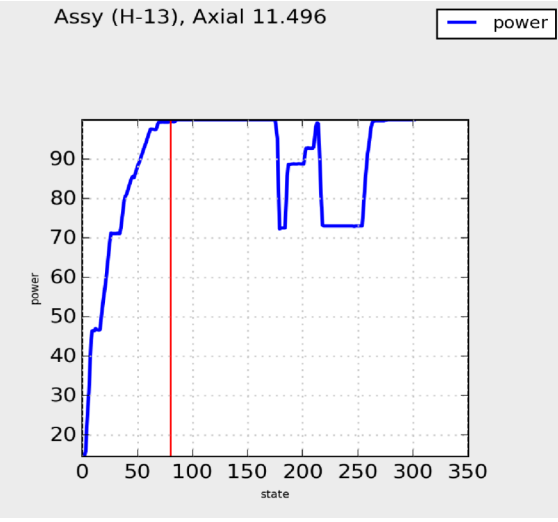
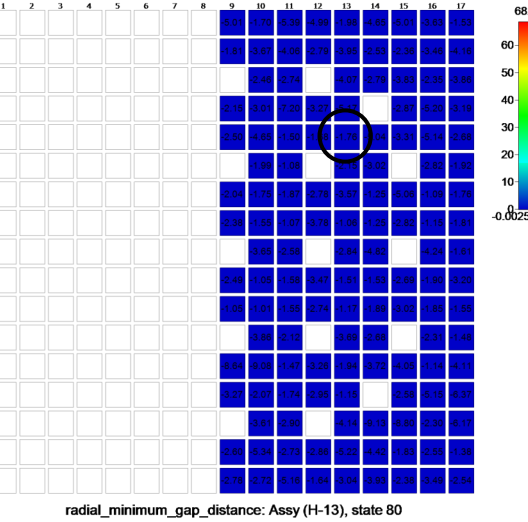
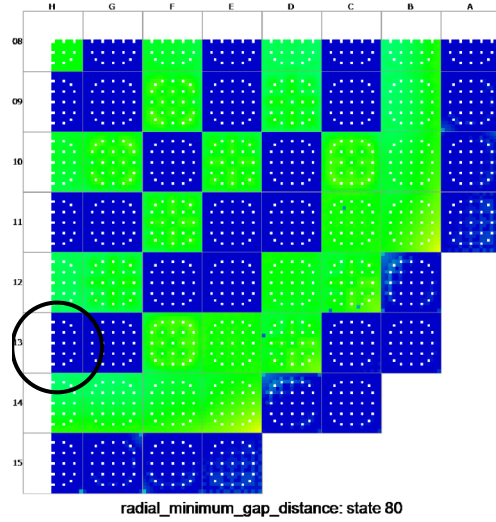
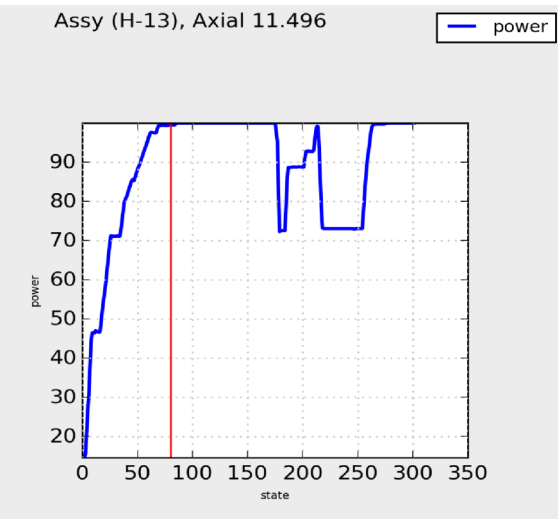
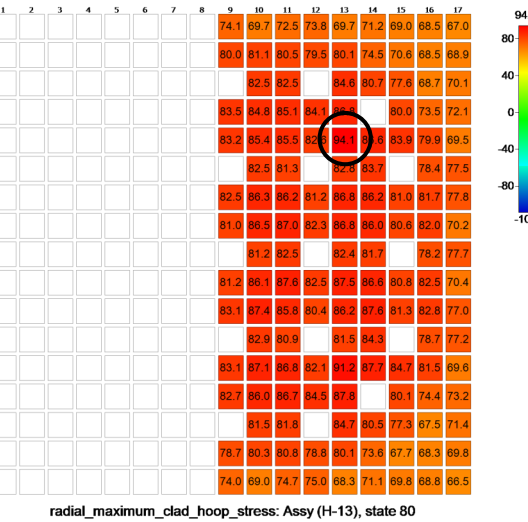
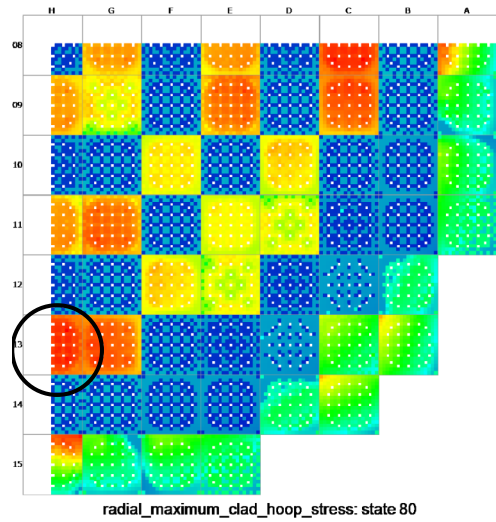


Figure 4.1: BISON predicted maximum clad hoop stress [MPa] (top) and minimum gap distance [ $\mu\text{m}$ ] (bottom) for start-up power ramp.

#### 4.1.2 Load-follow Ramp 1

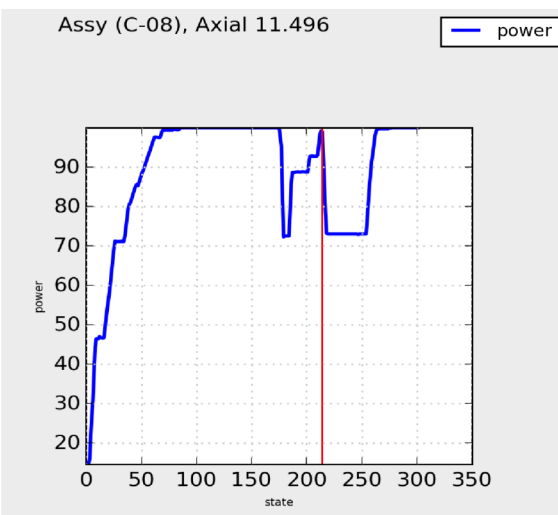
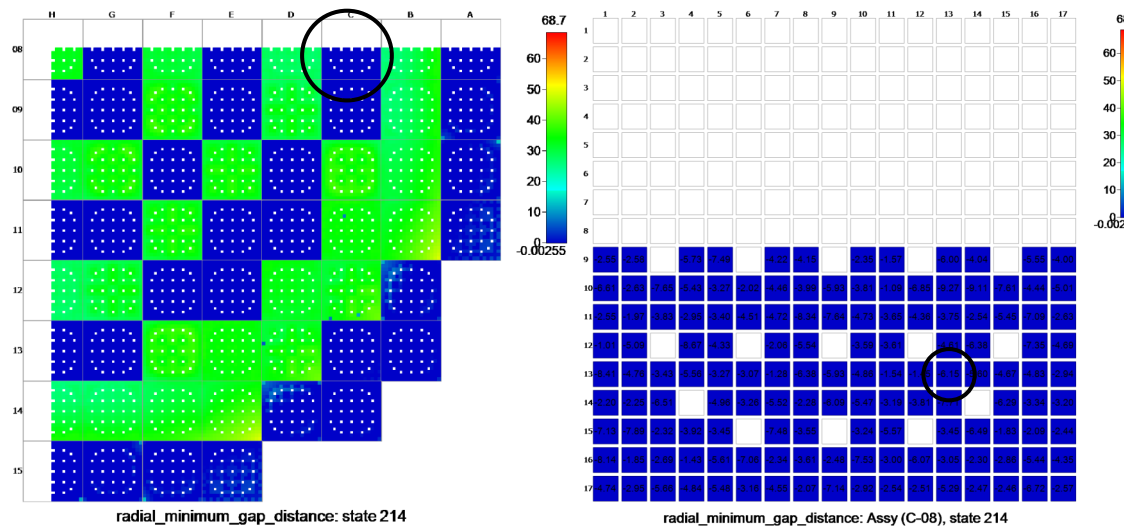
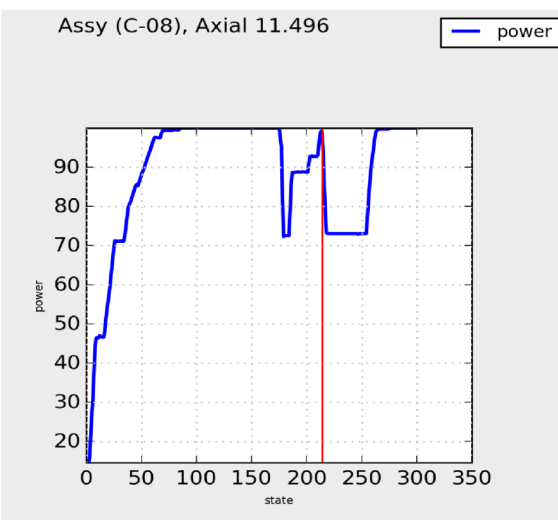
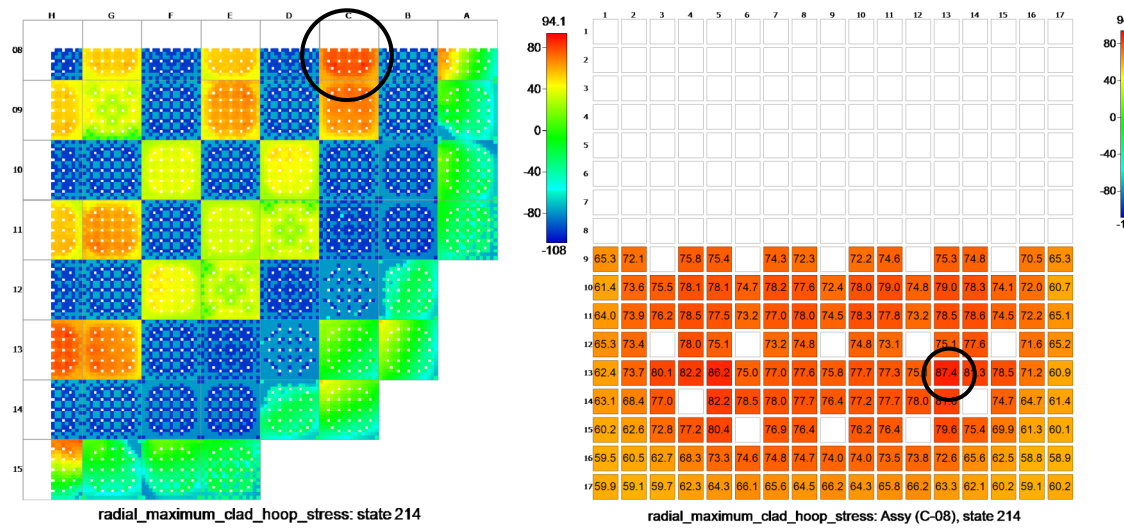


Figure 4.2: BISON predicted maximum clad hoop stress [ $MPa$ ] (top) and minimum gap distance [ $\mu m$ ] (bottom) for the first load-follow power maneuver.

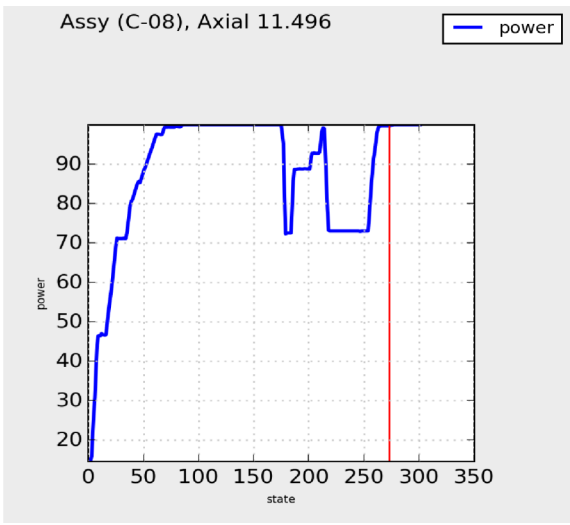
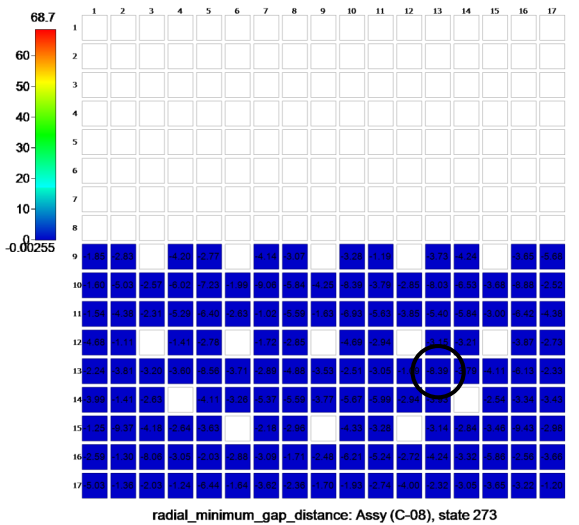
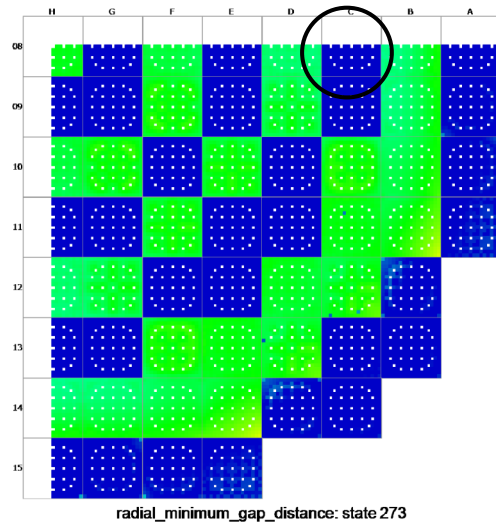
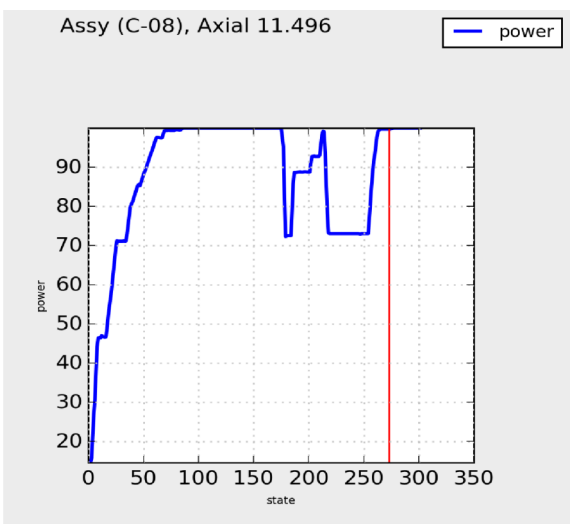
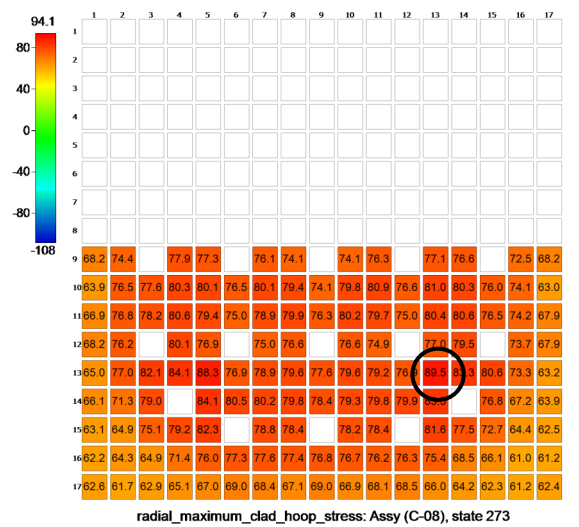
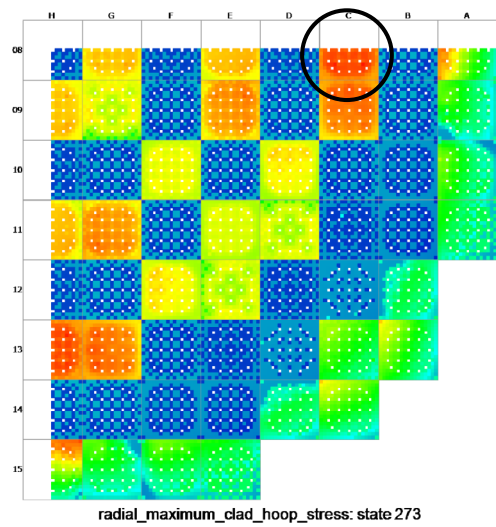


Figure 4.3: BISON predicted maximum clad hoop stress [MPa] (top) and minimum gap distance [ $\mu\text{m}$ ] (bottom) for the second load-follow power maneuver.

#### 4.1.3 Load-follow Ramp 2

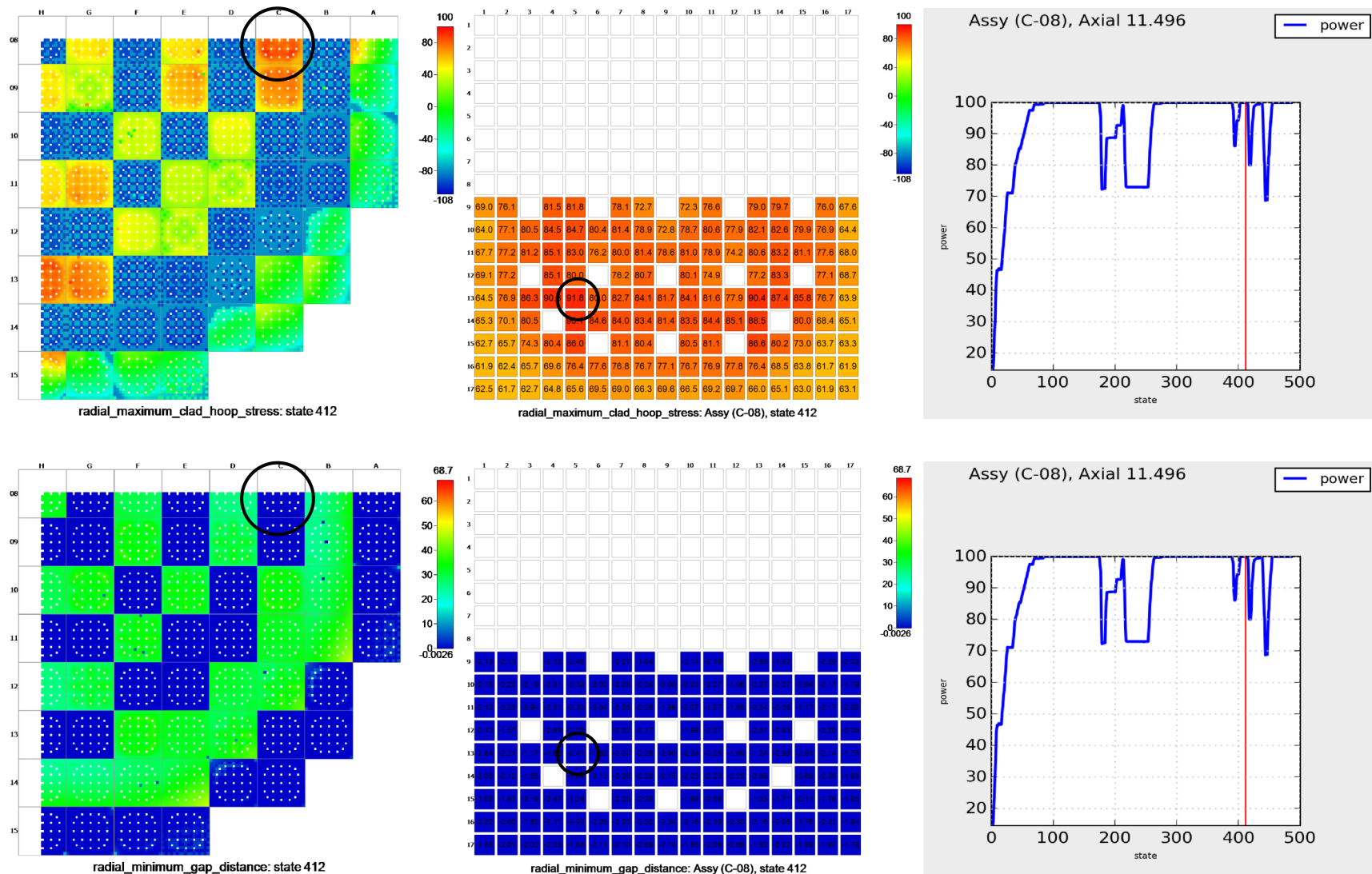


Figure 4.4: BISON predicted maximum clad hoop stress [MPa] (top) and minimum gap distance [ $\mu\text{m}$ ] (bottom) for the third load-follow power maneuver.

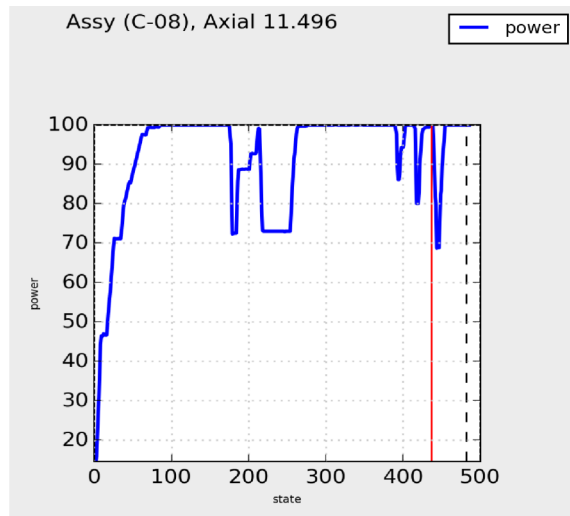
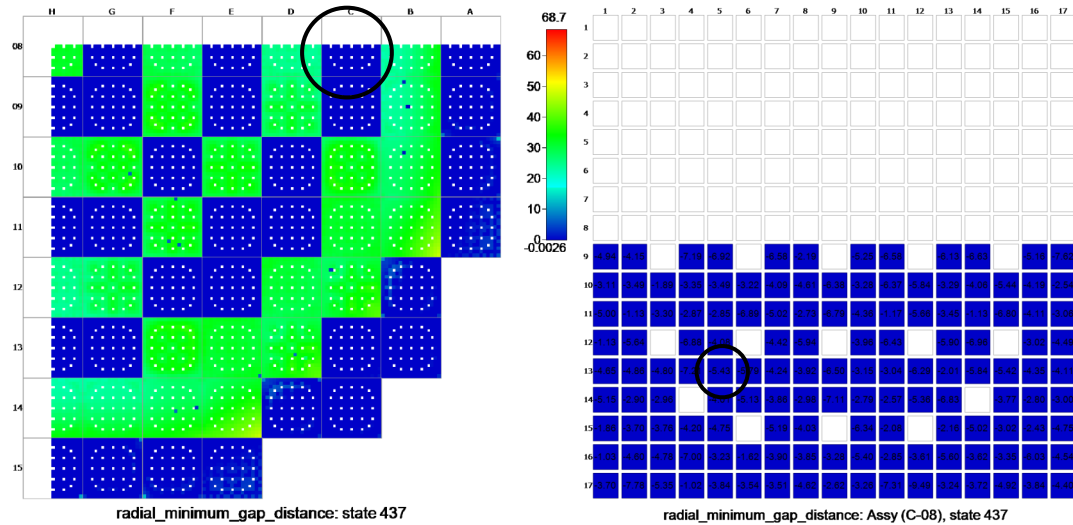
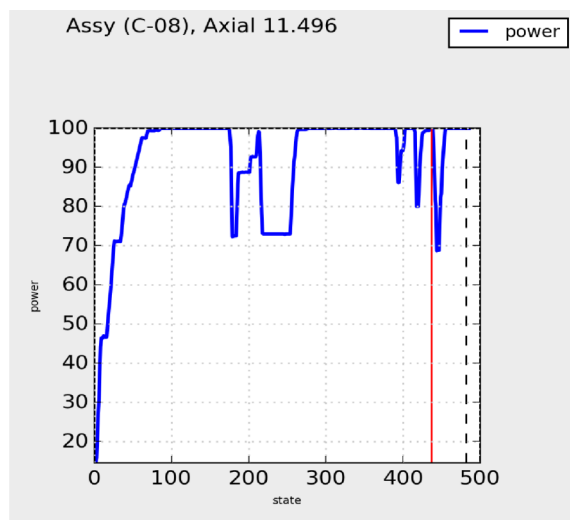
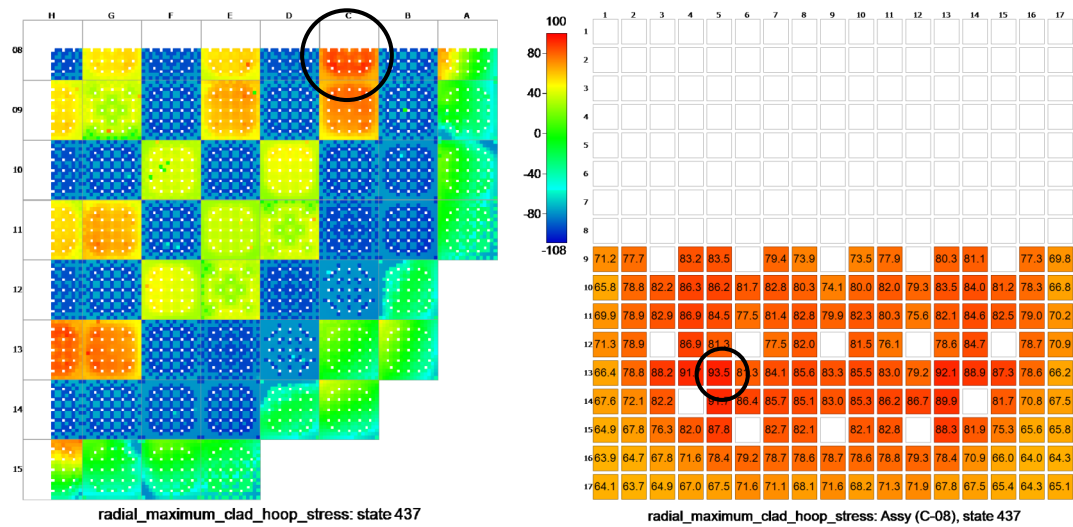


Figure 4.5: BISON predicted maximum clad hoop stress [MPa] (top) and minimum gap distance [ $\mu\text{m}$ ] (bottom) for the forth load-follow power maneuver.

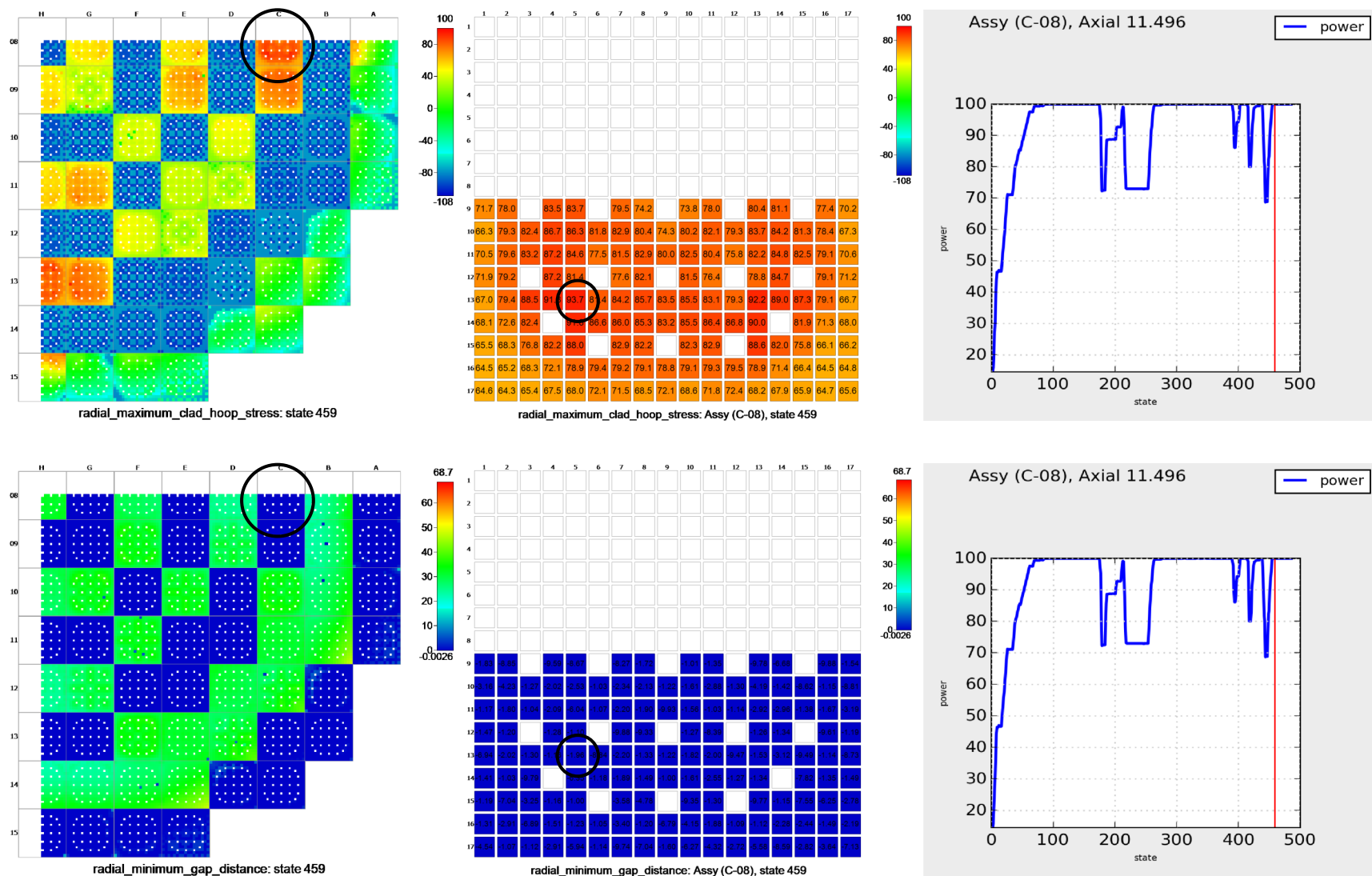


Figure 4.6: BISON predicted maximum clad hoop stress [ $MPa$ ] (top) and minimum gap distance [ $\mu m$ ] (bottom) for the fifth load-follow power maneuver.

#### 4.1.4 Load-follow Ramp 3

## 4.2 Limiting Pin

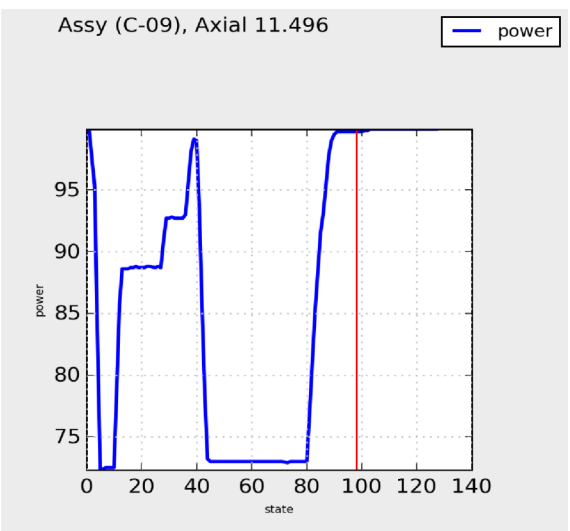
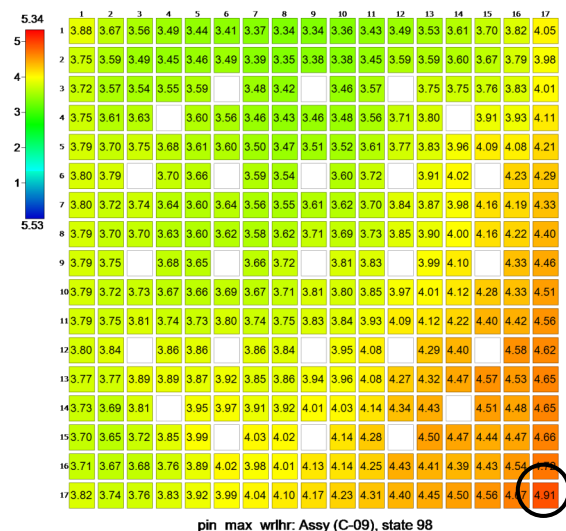
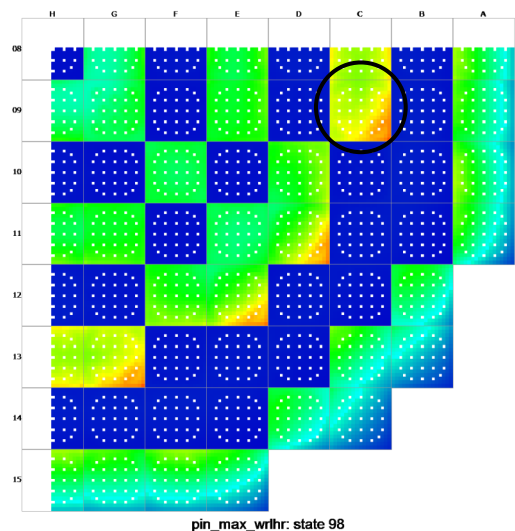
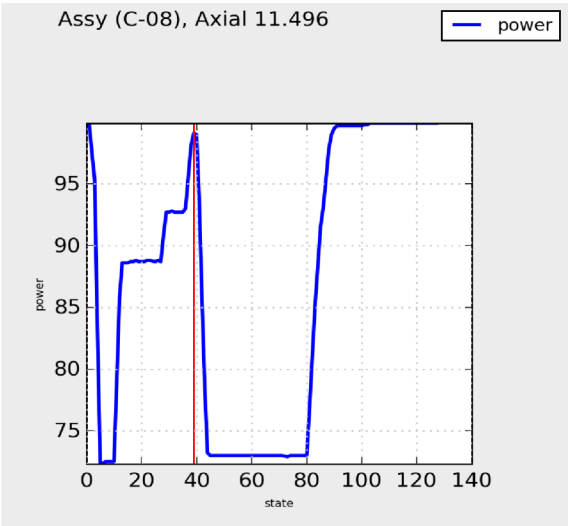
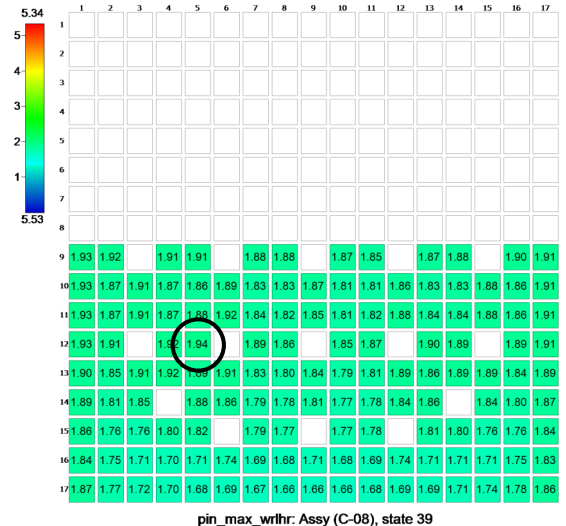
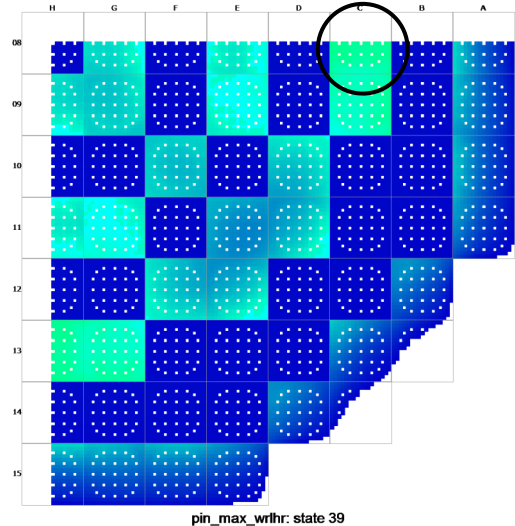


Figure 4.7: Weighted change in linear heat rate for the first (top) and second (bottom) load-follow power maneuver.

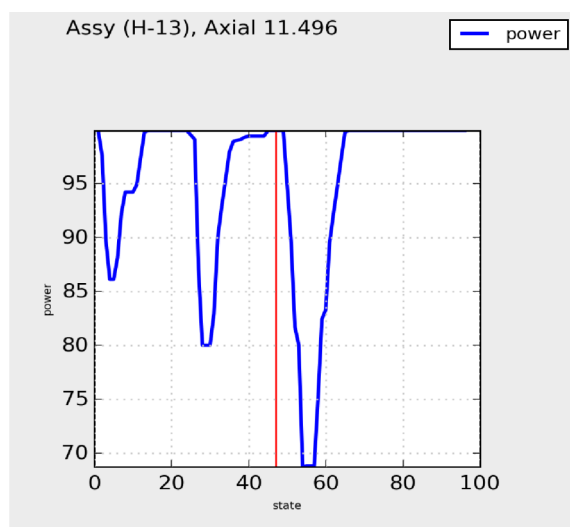
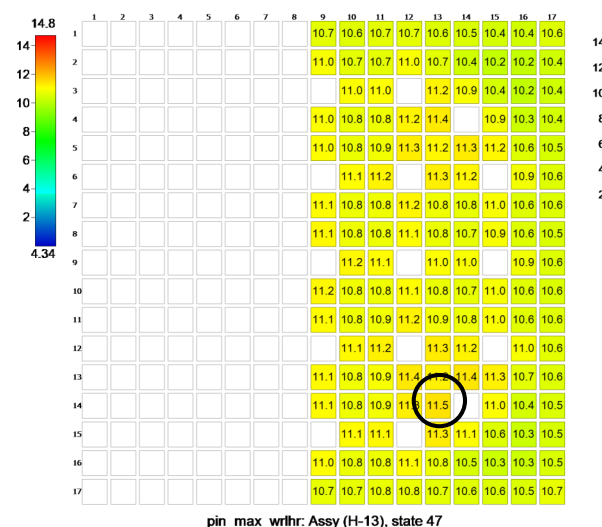
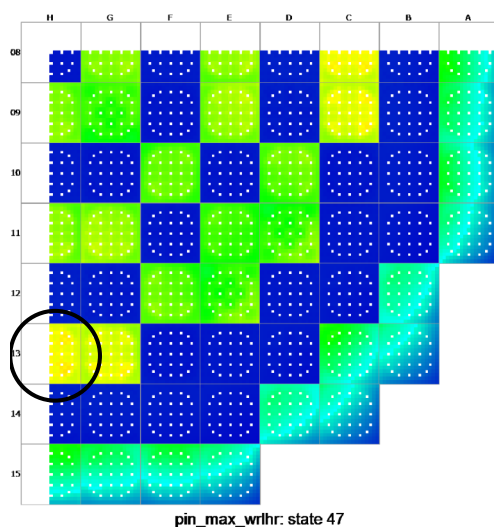
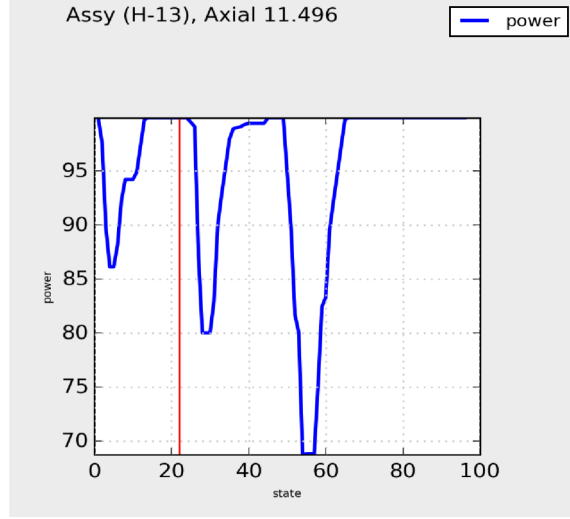
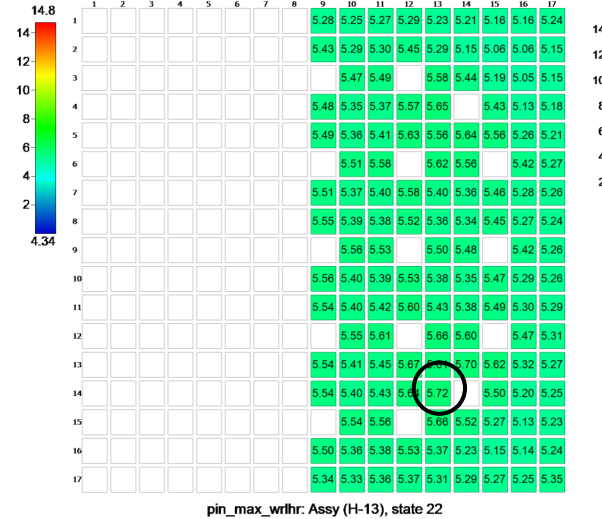
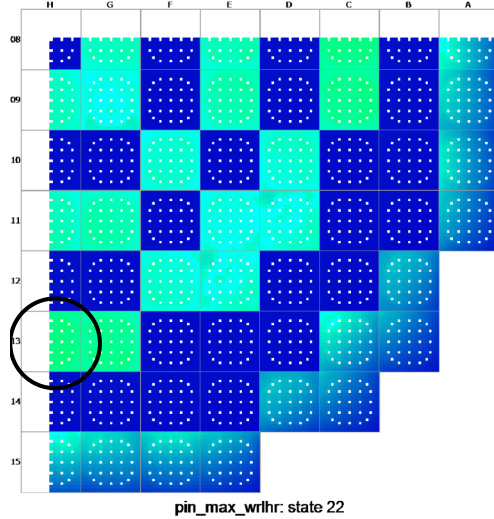


Figure 4.8: Weighted change in linear heat rate for the third (top) and forth (bottom) load-follow power maneuver.

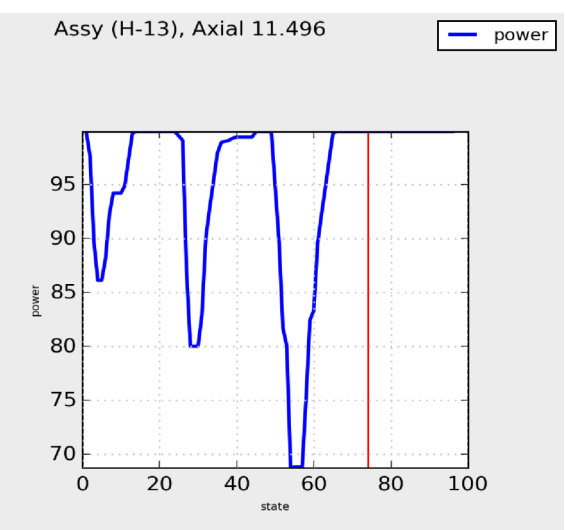
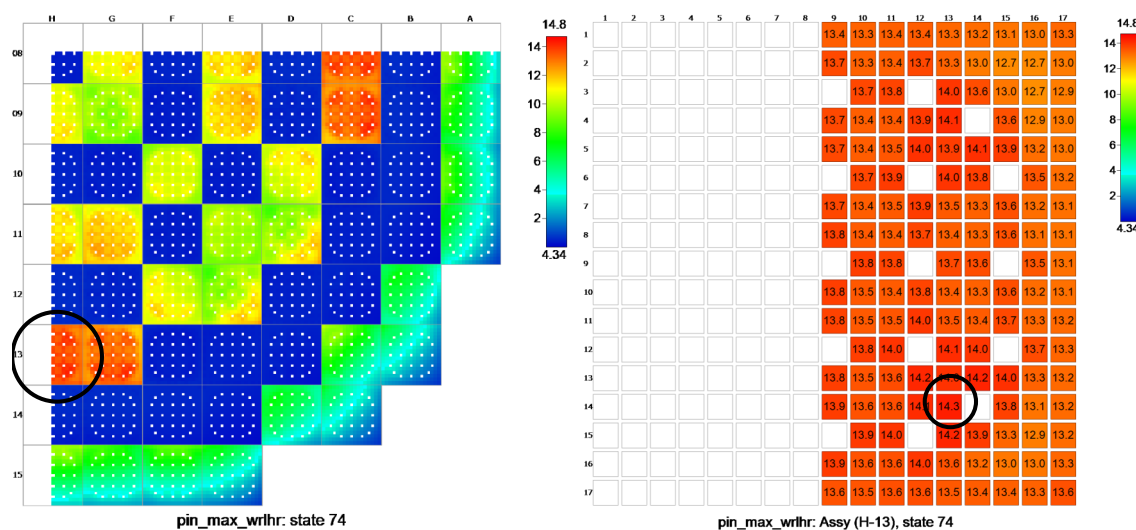
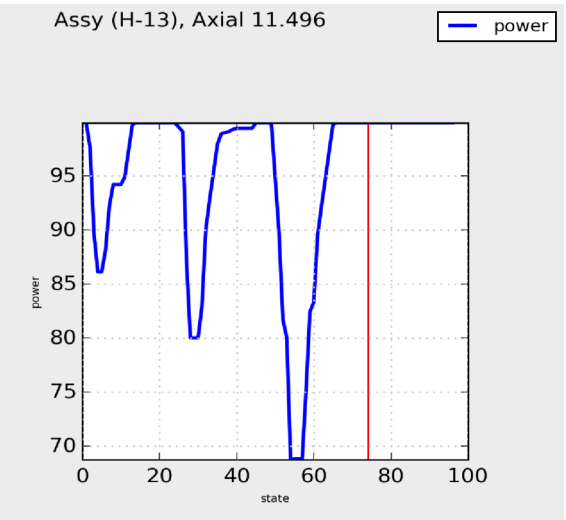
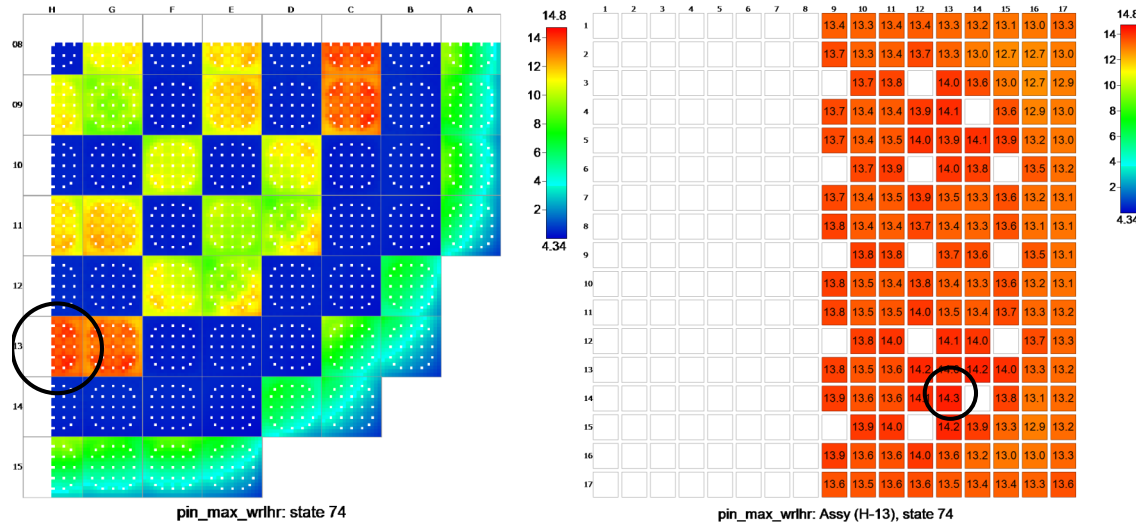


Figure 4.9: Weighted change in linear heat rate for the fifth (top) and forth (bottom) load-follow power maneuver.

## **Chapter 5**

# **Conclusions**

We conclude that graduate students like coffee.

# References

- [1] D. KOOK, J. CHOI, J. KIM, and Y. KIM, “Review of spent fuel integrity evaluation for dry storage,” **45**, 1, 115–124.
- [2] W. LYON, R. MONTGOMERY, J. RASHID, and S. YAGNIK, “PCI analysis and fuel rod failure prediction using FALCON,” in “Water Reactor Fuel Performance Meeting, Paris, France,” .
- [3] U.S ENERGY INFORMATION ADMINISTRATION, “Electricity data browser - Net generation for all sectors,” .
- [4] F. PARASCHIV, D. ERNI, and R. PIETSCH, “The impact of renewable energies on EEX day-ahead electricity prices,” **73**, 196–210.
- [5] A. LOKHOV, “Load-following with nuclear power plants,” **29**, 2, 18–20.
- [6] A. LOKHOV, “Technical and economic aspects of load following with nuclear power plants,” .
- [7] F. YOUSEFPOUR and M. B. GHOFRANI, “Improvement of the axial power distribution control capabilities in VVER-1000 reactors,” **27**, 10, 949 – 957.
- [8] P. SIPUSH, R. KERR, A. GINSBERG, T. MORITA, and L. SCHERPREEEL, “Load-follow demonstrations employing constant axial offset power-distribution control procedures,” **31**, 1, 12–31.
- [9] C. MEYER, C. BENNETT, D. HILL, and K. DZIKOWSKI, “Improved load follow strategy for return-to-power capability,” **41**, 1, 27–35.
- [10] M. GARTNER and J. LAVAKE, “POWER RAMP TESTING AND NON-DESTRUCTIVE POST-IRRADIATION EXAMINATIONS OF HIGH BURN UP PWR FUEL RODS,” pp. 27–38.
- [11] M. W. KENNARD, W. F. LYON, and A. T. MAI, “PCI Margin Analysis Methodology Using the Falcon Fuel Performance Code,” in “Proc. of Top Fuel 2016, Boise, ID, September 11-15, 2016,” .
- [12] N. CAPPS, R. MONTGOMERY, D. SUNDERLAND, M. PYTEL, and B. D. WIRTH, “Evaluation of missing pellet surface geometry on cladding stress distribution and magnitude,” **305**, 51–63.
- [13] B. COX, “Pellet-clad interaction (PCI) failures of zirconium alloy fuel claddinga review,” **172**, 3, 249–292.

- [14] L. O. JERNKVIST, “A model for predicting pellet-cladding interaction-induced fuel rod failure,” **156**, 3, 393–399.
- [15] R. MONTGOMERY, Y. RASHID, and A. ZANGARI, “FALCON Fuel Analysis and Licensing Code, Vol. 2, User’s Manual,” .
- [16] J. KILLEEN, E. SARTORI, and J. TURNBULL, “Experimental Data on PCI and PCMI within the IFPE Database,” in “Proceedings of Seminar on Pellet-clad Interaction in Water Reactor Fuels, Aix-en-Provence, France,” pp. 9–11.
- [17] N. APPS, M. KENNARD, W. LIU, B. D. WIRTH, and J. RASHID, “PCI analysis of a commercial PWR using BISON fuel performance code,” **324**, 131–142.
- [18] Y. ALESHIN, C. BEARD, G. MANGHAM, D. MITCHELL, E. MALEK, and M. YOUNG, “The effect of pellet and local power variations on PCI margin,” pp. 26–29.
- [19] M. OGUMA, “Cracking and relocation behavior of nuclear fuel pellets during rise to power,” **76**, 1, 35–45.
- [20] B. KOCHUNAS, B. COLLINS, D. JABAAY, T. J. DOWNAR, and W. R. MARTIN, “Overview of development and design of MPACT: Michigan parallel characteristics transport code,” in “Proc. of ANS M&C2015-Joint International Conference on Mathematics and Computation (M&C), Supercomputing in Nuclear Applications (SNA) and the Monte Carlo (MC) Method,” American Nuclear Society, 555 North Kensington Avenue, La Grange Park, IL 60526 (United States).
- [21] A. ZHU, B. COLLINS, B. KOCHUNAS, and T. DOWNAR, “Assessment of the Depletion Capability in MPACT,” in “PHYSOR 2014,” .
- [22] S. G. STIMPSON, B. S. COLLINS, and T. J. DOWNAR, “Axial transport solvers for the 2D/1D scheme in MPACT,” in “PHYSOR 2014,” .
- [23] M. AVRAMOVA, “CTF: A thermal hydraulic sub-channel code for LWR transient analyses,” .
- [24] M. GARTNER and G. FISCHER, “Survey of the power ramp performance testing of KWU’S PWR UO<sub>2</sub> fuel,” **149**, 1, 29–40.
- [25] S. G. STIMPSON, “Demonstration of Load-Follow Simulation with VERA-CS and Standalone BISON,” .
- [26] D. GASTON, C. NEWMAN, G. HANSEN, and D. LEBRUN-GRANDIE, “MOOSE: A parallel computational framework for coupled systems of nonlinear equations,” *Nuclear Engineering and Design*, **239**, 10, 1768–1778.
- [27] R. WILLIAMSON, J. HALES, S. NOVASCONE, M. TONKS, D. GASTON, C. PERMANN, D. ANDRS, and R. MARTINEAU, “Multidimensional multiphysics simulation of nuclear fuel behavior,” *Journal of Nuclear Materials*, **423**, 1, 149–163.
- [28] R. WILLIAMSON, K. GAMBLE, D. PEREZ, S. NOVASCONE, G. PASTORE, R. GARDNER, J. HALES, W. LIU, and A. MAI, “Validating the BISON fuel performance code to integral LWR experiments,” **301**, 232–244.

- [29] J. HALES, S. NOVASCONE, G. PASTORE, D. PEREZ, B. SPENCER, and R. WILLIAMSON, “BISON Users Manual, BISON Release 1.2.” .
- [30] R. O. MONTGOMERY, N. A. CAPPS, D. J. SUNDERLAND, W. LIU, J. HALES, C. STANEK, and B. D. WIRTH, “Advanced Pellet-Cladding Interaction Modeling Using the Us Doe Casl Fuel Performance Code: Peregrine,” *Transactions of the American Nuclear Society*, **110**.
- [31] R. GARDNER, S. STIMPSON, K. CLARNO, and R. PAWLOWSKI, “Review of Bison Usage in VERA,” .

# Vita

Juan Valdez was born....